Pure rotational R(0) and R(1) lines of CO in Ar baths: experimental broadening, shifting and mixing parameters in a wide pressure range versus ab initio calculations

M. yu. Tretyakov, E. A. Serov, D. S. Makarov, I.N. Vilkov, G.Yu. Golubiatnikov, T.A. Galanina, M.A. Koshelev, A. A. Balashov, A.A. Simonova, F. Thibault

Cite this: DOI: 00.0000/xxxxxxxxxx

Pure rotational R(0) and R(1) lines of CO in Ar baths: experimental broadening, shifting and mixing parameters in a wide pressure range versus *ab initio* calculations

M. Yu. Tretyakov,*[a] E. A. Serov[a], D. S. Makarov[a], I. N. Vilkov[a], G. Yu. Golubiatnikov[a], T. A. Galanina[a], M. A. Koshelev[a], A. A. Balashov[a], A. A. Simonova[b] and F. Thibault[c]

Received Date
Accepted Date

DOI: 00.0000/xxxxxxxxxx

Results of a rigorous study of the two first pure rotational transitions of CO perturbed by Ar are presented. The experimental part is based on the use of three different spectrometers covering together the pressure range from 0.02 up to 1500 Torr. The measurement results of collisional line shape parameters are supported by fully *ab initio* calculations, which are in remarkable agreement with retrieved data. A sub-percent uncertainty of line intensity measurements is achieved and the first firm evidence that the resonance spectrum of CO is observed on the continual pedestal is given. We analyze the results of our *ab initio* calculations on the basis of early analytical theories and demonstrate a good general applicability of the latter to the CO–Ar collisional system.

1 Introduction

One of the major goals of molecular spectroscopy is the development of a radiation propagation model, which is capable to cover a wide spectral range for various gas thermodynamic conditions. The information gathered in spectroscopic databases and well-developed theoretical methods allow modeling the observed spectra. In the spectral interval of a single line, the experimental data can be reproduced with a relative deviation down to about 0.1 % or even better. The wider the interval, the worse the agreement. In a broad range the spectra are usually simulated as a sum of individual line profiles representing resonant absorption and the so-called "continuum" or the non-resonant part. Such subdivision is rather arbitrary because all current line shape models are developed in the impact approximation, meaning that their validity range is limited to the vicinity of the line center [1,2]. Behavior of resonant line wings at large detuning from their center is still unknown, so this part of resonant absorption is commonly included in the continuum [3]. Another component of the continuum is bimolecular absorption (as a particular case of "supermolecular absorption" within the range of validity of the binary collision approximation), i.e. the absorption caused by the dipole moment of two molecules collisionally interacting with each other [4]. This absorption, in turn, can be divided into the components corresponding to free molecular pairs, stable (true bound), and metastable (quasibound) dimers [5,6]. Relative fraction of these components is significantly different for various molecular pairs under chosen thermodynamic conditions. For example, it was demonstrated [7–10] that the contribution of bound dimers to the continuum is significant for H_2O–H_2O pairs in the millimeter and submillimeter wavelength ranges even at room temperature. The same has been proved for CO_2–CO_2 and even CO_2–Ar pairs [11–13]. However, the free pair component is dominating for the N_2–N_2 continuum and the dimeric part is negligible [14]. The contribution of resonant line wings to the continuum remains one of the oldest unsolved problems in molecular spectroscopy [15–18]. The solution of the problem is additionally complicated by insufficient accuracy of the resonant line parameters distorting the continuum spectrum [19]. To break through this challenge, a thorough investigation of line shape is necessary, including the range of frequency detuning from the line center where the impact approximation becomes no longer valid. The detuning should be thus comparable to or even larger than $1/2\pi\tau_c$, where τ_c is a molecular collision duration, which is about 0.1–1 ps [1,20] and, therefore, the requested detuning should be at least 1–10 cm^{-1}. The line shape analysis within such enormous range is possible if (i) the spectrum is not dense and (ii) the gas pressure is high enough, so the lines are quite broad and their wings can be traced far away from the center but triple collisions can be still neglected.

Simple molecular systems are preferable for such an investigation because accurate interpretation of experimental spectra over a quite large spectral interval requires the support of quantum dynamics methods that are difficult to handle for relatively large molecules. As an example of such investigations we note the work [21], where the manifestation of super- and sub-Lorentzian

[a] *Institute of Applied Physics, Russian Academy of Sciences, 46 Ulyanov str., Nizhny Novgorod, 603950, Russia; *E-mail: trt@ipfran.ru*
[b] V.E. Zuev Institute of Atmospheric Optics SB RAS, Tomsk, 634055, Russia
[c] Univ Rennes, CNRS, Institut de Physique de Rennes, UMR 6251, F-35000, Rennes, France

wings of HCl lines together with collisional line mixing effect were suggested for ro-vibrational spectra modeling. In the present study we choose regular well-spaced lines of a pure rotational spectrum (to exclude the influence of vibrational excitation) of the most abundant isotopologue of carbon monoxide in argon baths. This spectrum has been studied extensively both experimentally and theoretically and is thus rather well known. Line positions are known with sub-kHz accuracy from Lamb-dip measurements[22]. Pressure broadening, shifting and "wind effect" (speed-dependence of collisional relaxation) of pure rotational lines were extensively studied[23–27]. The effect of collisional coupling leading to mixing of CO lines was investigated for the fundamental rovibrational[28] and the first overtone bands[29]. To the best of our knowledge, the shape of rotational lines of the CO spectrum was not investigated at elevated (close to atmospheric and above) pressures, except for the previous work[30] dedicated to the R(0) line, hereafter referred to as Paper I, and to which some of us have contributed. In Paper I, the observed shapes of this line were compared with *ab initio* calculated profiles and a sub-percent agreement was demonstrated. However, in that work experimental line parameters were not reported. In the present paper, we focus on the analysis of experimental recordings obtained for the R(0) line of $^{12}C^{16}O$ molecule presented in Paper I and report similar spectra for the R(1) rotational transition.

Similarly to Paper I, we employ three different, on the principle of operation, spectrometers with complementary abilities covering the pressure range from about 20 millitorr up to 1500 Torr. Note that the Doppler broadening can be neglected in most part of this range of pressures because of relatively low transition frequencies. This allows us to simplify the consideration of the Dicke narrowing and the correlations between velocity changing and dephasing molecular collisions, which mask the manifestation of other collisional effects on the shape of lines in the infrared range. This gives us a unique opportunity for continuous tracing of the molecular line shape and its parameters variation under conditions changing from highly rarified to quite dense gas. Spectra recorded with a video spectrometer, a spectrometer with radioacoustic detection (RAD) and a resonator (cavity) spectrometer were used to study line shape and to retrieve line parameters. The simultaneous use of three spectrometers allows revealing and reducing potential systematic instrumental errors in each of them. The available range of frequency detuning from the line center is about 40 times the half width at half maximum (HWHM) at room temperature and atmospheric pressure and reaches about 3 cm^{-1}, which is close to the limit of the impact approximation validity. So, one of the goals of this study is to verify whether we can observe the manifestation of the effects beyond the impact approximation and/or bimolecular component of gas absorption.

The collisional parameters retrieved from experimental recordings of the R(0) and R(1) lines having up to several thousand signal-to-noise ratio (SNR) are compared with the results of quantum scattering calculations[30–34] using highly accurate *ab initio* interaction potentials[35,36]. We omit the details of these calculations in the present work and address the interested reader to the aforementioned previous publications.

The structure of the paper is the following. Section 2 contains a brief description of the experimental details and spectral analysis procedure. In Section 3 we analyze the uncertainty of the line shape coefficients obtained from different spectrometers recordings and compare these results with each other, with parameters derived from *ab initio* calculations and with other theoretical and experimental data. In Section 4 we discuss some relevant problems of line shape modeling in the context of our results. Our findings are summarized in the Conclusions. The temperature dependence of the collisional broadening of the lines under study is discussed in Appendix.

2 Experimental techniques and data processing

The information on our spectrometers can be found in Paper I and references therein. In this Section the detailed description of the spectra analysis procedure is given for each spectrometer.

2.1 Video spectrometer

The video spectrometer[37,38] was used to obtain line profile recordings at pressures within 20–300 mTorr in pure CO and CO–Ar mixtures. Two cylindrical gas cells with a length of 200 cm and 134 cm and 10 cm in diameter were used for the recordings of the R(0) and R(1) lines, respectively. The R(0) line was recorded using frequency manipulation (FM), that is low frequency (80 Hz in our work) modulation using a square-wave modulating function with precisely known deviation of frequency, both in pure CO and in mixtures with argon. The R(1) line was recorded using 100 % amplitude modulation (AM) for pure CO and FM for CO–Ar mixtures. The typical number of frequency points per recording was 501. All recordings were made at controlled room temperature varying from day to day within the 298–300 K range. Temperature variations did not exceed ± 0.5 K during a pressure ramp experimental cycle. The number of recorded spectra and the experimental pressure range are listed in Table 1.

The baseline contribution to the output signal of the video spectrometer is significant. The baseline signal was recorded separately in the empty cell for each series of recordings. It was interpolated with a smooth function and subtracted from the FM recordings at all pressures before further processing of the spectra. A typical series of FM and AM spectra recordings is presented in Figs. 1-2.

Table 1 Experimental details for the study by means of the video spectrometer.

Line	Gas	Pressure range, Torr	Number of spectra	Path length, cm
R(0)	CO	0.038–0.207	24	400
R(0)	CO+Ar	0.030–0.191	64	400
R(1)	CO	0.031–0.267	11	134
R(1)	CO+Ar	0.020–0.191	109	134

The line shape model $LS(\nu)$ is an Hartmann-Tran profile (HTP)[39] in its several familiar limits corresponding, in particular, to the Voigt profile (VP), the quadratic speed-dependent Voigt profile (qSDVP), and the quadratic speed-dependent Rautian profile (qSDRP) in case of the AM mode, while for the FM mode we used:

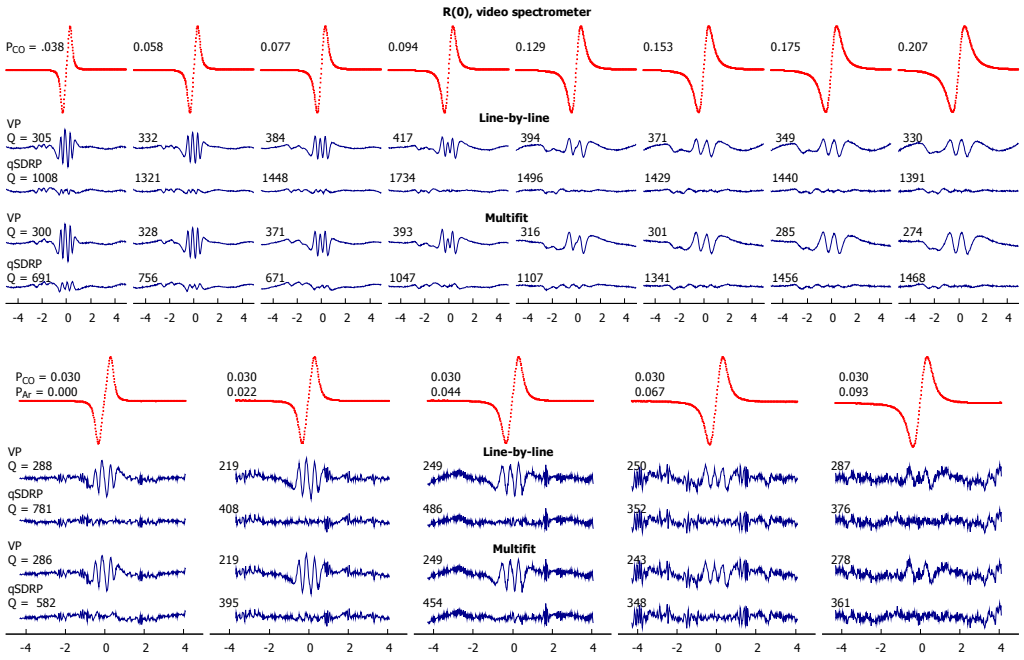

Fig. 1 Typical series of video spectrometer recordings of the R(0) line (red points) in pure CO (upper panel) and CO–Ar mixtures (lower panel) and "obs.–calc." residuals of the VP and qSDRP (dark blue traces) fit to the recordings for both line-by-line and multispectrum fit. For better visibility, residuals are multiplied by a factor of 30. Gas pressures and fit quality factors Q (ratio of the line amplitude to the standard deviation of the fit residual) are shown near the corresponding traces. X axis is the frequency detuning from the fitted central frequency value in MHz.

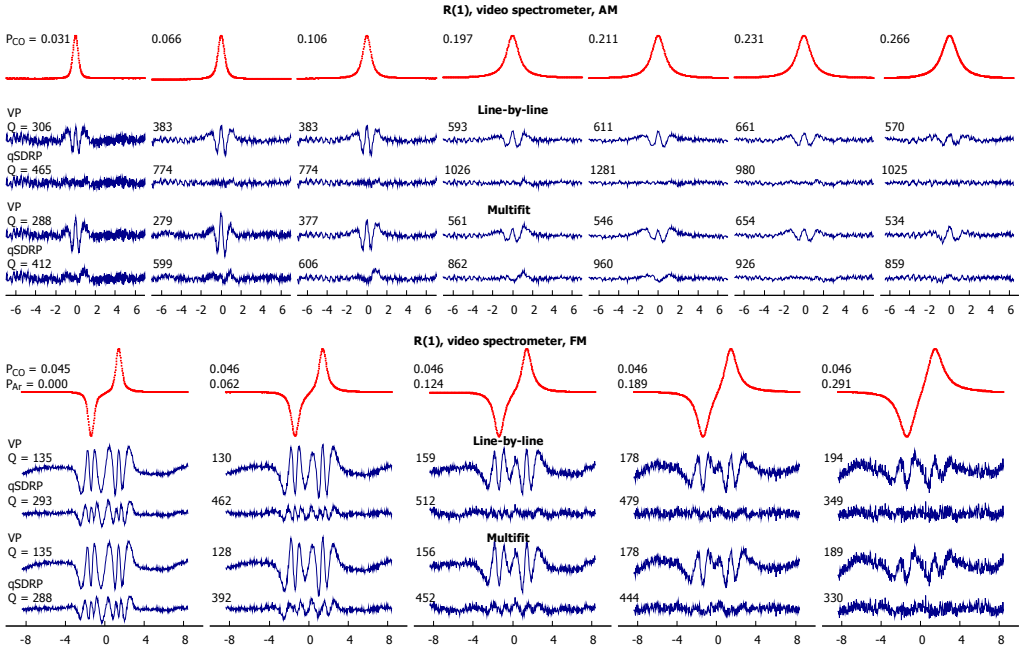

Fig. 2 Same as Fig. 1, but for the R(1) line.

$$LS_{\mathrm{FM}}(\nu) = LS(\nu - D) - LS(\nu + D), \quad (1)$$

where D is the (known) preset value of frequency deviation used for line recording. The Doppler width of the line was calculated for each series and fixed in the fit. It is known that a backward wave oscillator (BWO) used as a radiation source in the experimental setup generates overtones of the main frequency[40]. The first CO lines are nearly equidistant, so the overtones cause an additional absorption signal in the frequency ranges close to the studied line center (see, e.g., Fig. 16–6 from Townes[41] or Fig. 1 from Burrus et al.[42]). For R(0) line recordings, this corresponds to the extra absorption signal related to the R(1) line, and for R(1) line recordings to the R(3) line. Note that the second harmonic (the first overtone) of the BWO frequency is the only noticeable harmonic in our case, having a relative power of 1–0.1 %. This extra absorption signal was noticeable and taken into account by introducing to the model function a line profile with fixed parameters corresponding to the line excited by the overtone frequency. The amplitude of this line was adjusted for each separate recording series, because the efficiency of the overtone generation and the corresponding signal might vary depending on the radiation reflections in the cell.

Two widely used procedures were employed for the retrieval of pressure independent line shape coefficients, namely, (i) “line-by-line fitting" of individual recordings with further approximation of obtained line shape parameters by expected pressure dependences, and (ii) “multispectrum fitting” (or just “multifit”), when the line shape model is optimized simultaneously to all recordings in a series of measurements. The former method allows a more detailed analysis of experimental data (e.g., revealing systematic deviations from expected pressure dependences), but the latter is considered to be more reliable because the expected dependences included in the model reduce the freedom of the fit and the correlation between the adjustable parameters.

The required line shape parameters and their expected dependence on pressure P should be:

$$\nu_c = \nu_0 + \Delta_w = \nu_0 + \delta_w P, \quad (2)$$

$$\Gamma_{w,\Omega_R} = \sqrt{\Gamma_w^2 + \Omega_R^2} = \sqrt{(\gamma_w P)^2 + \Omega_R^2}, \quad (3)$$

$$\Gamma_w = \gamma_w P + k^2 \cdot D_0 / P, \quad (4)$$

$$\Gamma_2 = \gamma_2 P, \quad (5)$$

where ν_c is the line center frequency; ν_0 is the transition frequency at zero pressure; Δ_w is the line center pressure shift; w is either for V or 0; Δ_V, Δ_0, Γ_V, Γ_0 and Γ_2 are conventional shift and half-width parameters for VP and qSDVP models, respectively (Δ_2 parameter is set to 0 in the model for all spectra); δ_V, δ_0, γ_V, γ_0 and γ_2 are the corresponding pressure independent line shape coefficients; Γ_{w,Ω_R} is the effective half-width parameter to take into account the effect of transition saturation by radiation power; Ω_R is the Rabi frequency quantifying the transition saturation[41]; $k = 2\pi/\lambda$ is the wavenumber and D_0 is the molecular diffusion coefficient, so the term $k^2 D_0/P$ takes into account the collisional confinement of the active molecules, known as the Dicke narrowing effect (eq. III.19 in Hartmann et al[1]). The latter is assumed to influence noticeably the line shape at low pressures typical for the video spectrometer. We expected that modeling the saturation and Dicke narrowing can cause similar features in the half-width pressure dependence at low pressures, meaning that the parameters characterizing these effects can be strongly correlated and, therefore, should not be adjusted simultaneously. To avoid the problem, radiation power was strongly attenuated in the experiments with the video spectrometer. The intensity of the radiation beam (close to Gaussian) was further reduced by expanding the beam into a gas cell with a diameter of 10 cm. The Rabi frequency was estimated to be less than 10 kHz; therefore, the corresponding impact on the line shape can be neglected. Based on this, Ω_R was fixed to zero during processing of the video spectrometer data.

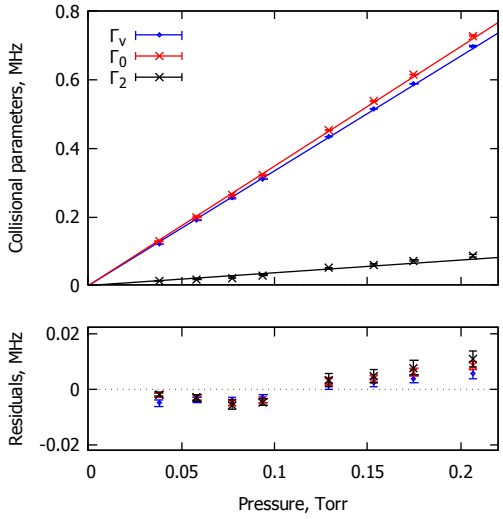

Fig. 3 Upper panel: Pressure dependence of Γ_V, Γ_0 and Γ_2 parameters of the R(0) line at 296 K in the case of self-broadening, obtained from the video spectrometer recordings and the VP and qSDRP. Fitted linear ($y = ax$) dependences are shown by solid lines. Lower panel: Deviations from the linear dependence of the parameters plotted in the upper panel. Error bar corresponds to three standard deviations of the fit (3σ).

The remaining influence of the spectrometer baseline was revealed. Both multiplicative and additive polynomials (up to the quadratic with frequency terms) were used in the model function to take this influence into account. The baseline parameters and scaling factor for the line amplitude were independent and variable for each recording. The calculated line intensity from HITRAN2020[43] was used to take into account the radiation path length through the Bouguer-Beer-Lambert law.

In the line-by-line fitting procedure, parameters of the model profile corresponding to certain pressure and temperature are retrieved for each recording. The usage of the VP model reveals in the residual the characteristic speed-dependence (SD) related features of the line shape (Figs. 1–2). Using the qSDVP or the qSDRP model improves the fit quality (Q is the ratio of the maximum signal to the residual standard deviation) by a factor of 2 to 4, indicating that the manifestation of the SD and/or Dicke effect is rather weak in these spectra. In this case, the retrieved

Γ_2 values might be biased due to mutual correlation of multiple adjustable parameters of the model. The potential biasing of line width related parameters is illustrated in Fig. 3, which shows a simultaneous insignificant systematic deviation (observed only in the residuals, but still exceeding the statistical uncertainty of the measurements) of all retrieved Γ_V, Γ_0 and Γ_2 parameters from the expected linear dependence. Recordings in CO–Ar mixtures also show the manifestation of non-Voigt effects, but the SNR is less in this case and potential systematic error of this kind is hidden. Note that, for the analysis of recordings in CO–Ar mixtures, Eqs. (2-5) were modified in the usual way using the binary collision approximation to take into account different efficiency of CO–CO and CO–Ar collisions.

The SNR of the video spectrometer recordings and related pressure interval are insufficient for unambiguous simultaneous retrieval of (mutually correlated) line shape parameters responsible for both the SD and the Dicke effect. In these conditions the common strategy suggests fixing the Dicke effect parameter in the fitting line shape model. Recall that in the qSDRP the corresponding parameter is called the velocity-changing collision rate ν_{VC}. As an upper value of this parameter (or an initial value in the fitting procedure) ν_{diff} is often used which is deduced from the mass diffusion coefficient D_0 via $\nu_{diff} = k_B T/2\pi m D_0$, where m is the mass of the optically active molecule. The value of $\nu_{diff} = 0.926$ MHz/Torr for CO in Ar at 299 K was reported in the earlier work[44]. Significantly smaller values of the velocity changing collision rates, namely 0.301 MHz/Torr for the R(0) line in Paper I[30] and 0.334 MHz/Torr for the R(1) line in the present work were calculated *ab initio* for 297.5 K as the real part of the complex Dicke parameter ν_{opt} (see eq. (A.4) from Paper I for details). We used these *ab initio* values as fixed parameters of the qSDRP model at the first stage of the experimental data treatment within the line-by-line fitting procedure. Note that the 100 % variation of this parameter did not produce a noticeable impact on the residuals of the fit, but at the same time affected the retrieved Γ_0 and Γ_2 parameters. Moreover, it was found that the variation of ν_{VC} affects the linearity of the pressure dependence of Γ_2. Numerical simulation of experimental data fitting also confirmed that the use of improper value of ν_{VC} leads to the nonlinear pressure dependence of the retrieved Γ_2 values. So, at the next step of the experimental data treatment, the ν_{VC} value was manually adjusted to achieve the best possible linearity of Γ_2 versus pressure for all available data. The obtained value of ν_{VC} was further refined in the iterative procedure after similar treatment of experimental data from the RAD spectrometer. The final values of 0.151 and 0.167 MHz/Torr were used in the multispectrum fitting procedure for the R(0) and R(1) lines, respectively. Note that a similar significant deviation between the experimental ν_{VC} values and *ab initio* results was reported for the CO–Ar collisional system for several fundamental band lines[36].

The result of multifit applied to the same series of recordings is shown in Figs. 1–2. As expected, the residuals between observed and calculated spectra related to the individual recordings are somewhat worse than in the case of line-by-line fitting. In the case of more than one series of recordings, the weighted averaged over these series value was taken.

The final values of the parameters retrieved from these spectra are given in Table 2. All values are recalculated to the temperature of 296 K as detailed below. Shifting coefficients are not reported as not reliably determinable from these spectra. They were estimated to be smaller than ± 20 kHz/Torr for both lines for self- and Ar-broadening cases.

Table 2 Line shape coefficients, in MHz/Torr, for the R(0) and R(1) lines at 296 K from the video spectrometer recordings. One standard deviation of the parameter value obtained from the fit is given in parenthesis.

Line	Gas	Coef.	Line-by-line	Multifit
R(0)	CO	γ_V	3.334(9)	3.333(1)
		γ_0	3.478(11)	3.454(2)
		γ_2	0.358(14)	0.303(2)
	Ar	γ_V	2.728(10)	2.737(4)
		γ_0	2.811(27)	2.785(5)
		γ_2	0.291(10)	0.266(9)
R(1)	CO	γ_V	3.269(9)	3.267(2)
		γ_0	3.370(12)	3.374(2)
		γ_2	0.312(16)	0.302(3)
	Ar	γ_V	2.641(5)	2.637(44)
		γ_0	2.761(16)	2.799(77)
		γ_2	0.484(10)	0.519(100)

Note that the aforementioned empirical adjustment of ν_{VC} does not completely resolve the problem of the correlated nonlinear behavior shown in Fig. 3. As a probable origin of such a behavior we point to the potential nonlinearity of converting radiation power to output signal by the point-contact semiconductor radiation detector used in the video spectrometer for these measurements. This problem can arise if the voltage-current characteristic of the detector is not a perfectly quadratic function even at small radiation power levels utilised in the present work.

2.2 RAD spectrometer

The radioacoustic spectrometer[45–48] was used for recording the R(0) and R(1) line profiles in the pressure range from several dozen of mTorr up to several Torr at room temperature (the cell temperature was stabilized by the active thermostat within $\sim$0.5 K). These recordings contained 201 or 151 frequency points, but due to the high stability of temperature and pressure in the short 10-cm gas cell (which is much simpler to implement than in the 2-m video cell), multiple recordings were performed with averaging of the recorded spectra. The number of the averagings varied from 8 for the highest pressures (stronger signal) up to 24 for the lowest ones (weaker signal). FM mode was used in all cases.

Table 3 Experimental details for the study by means of the RAD-spectrometer.

Line	Gas	Pressure range, Torr	Number of spectra
R(0)	CO	0.021–1.25	44
R(0)	CO+Ar	0.027–2.05	50
R(1)	CO	0.060–2.98	30
R(1)	CO+Ar	0.107–3.00	23

Recordings of the R(0) line were processed as follows. At the stage of the data acquisition, the synchronous detection phase was adjusted for each recording in order to obtain a maximum signal in one of the two recording channels shifted in phase by $\pi/2$[49]. No extra signals corresponding to the overtone of BWO frequencies were revealed. The baseline contribution to the total signal was near 10^{-4} of the maximum signal amplitude. The same VP and qSDRP (with fixed ν_{VC} and $\delta_2 = 0$) line shape models together with the same expected pressure dependences Eqs. (2), (3) and (5) (and their analogs for spectra of gas mixtures analysis) were used as for the video spectrometer recordings. The Rabi frequency value was evaluated from the BWO power and the cell diameter as 0.13±0.05 MHz, in a good agreement with 0.16–0.17 MHz retrieved from fits. The maximum fit quality for the R(0) line recordings reached ~ 12000 for the qSDRP model, which almost corresponds to the limit determined by instrumental noise. A typical example of experimental recordings is given in Fig. 4 together with the results of the fitting procedures.

The following complications accompanied the R(1) line study. A weak manifestation of the R(3) line interacting with the overtone of BWO radiation was observed and the corresponding profile (fixed width and position and free amplitude) was added to the fitting function. To decrease the influence of the molecular transition saturation effect, the BWO power was attenuated by a factor of 10, and the radiation source was placed at the longest possible distance from the cell, which also decreased the power. This reduces the SNR, but minimizes systematic errors in the collisional parameters retrievals. The retrieved from fits Rabi frequency was within 0.04–0.06 MHz.

The influence of the baseline was found to be stronger than for the R(0) recordings, at pressures above 0.6 Torr (up to 10^{-3} from the maximum signal amplitude). Even the cubic polynomial in the model function was not satisfactory to remove the baseline influence. To resolve this problem, it was decided not to increase the degree of the polynomial but to determine the baseline experimentally. The cell was filled by non-absorbing gas (Ar) and the obtained signal was subtracted from the spectra in the same way as for the video spectrometer recordings.

A typical example of the obtained spectra is given in Fig. 5 for one pressure ramp series together with the result of the fitting procedures. The final values of the parameters retrieved from these spectra and rescaled at 296 K as for the video spectrometer are given in Table 4.

Table 4 Line shape coefficients, in MHz/Torr, for the R(0) and R(1) lines at 296 K from the RAD spectrometer recordings. One standard deviation of the parameter value obtained from the fit is given in parenthesis.

Line	Gas	Coef.	Line-by-line	Multifit
R(0)		γ_V	3.423(4)	3.415(6)
		δ_V	–0.0032(2)	–0.0032(3)
	CO	γ_0	3.475(5)	3.470(4)
		γ_2	0.322(4)	0.319(4)
		δ_0	–0.0039(8)	–0.0034(5)
		γ_V	2.738(7)	2.734(7)
		δ_V	–0.0047(2)	–0.0056(9)
	Ar	γ_0	2.773(9)	2.778(8)
		γ_2	0.281(5)	0.277(9)
		δ_0	–0.0043(5)	–0.0059(14)
R(1)		γ_V	3.313(5)	3.292(10)
		δ_0	–0.007(1)	–0.005(2)
	CO	γ_0	3.378(2)	3.372(16)
		γ_2	0.325(4)	0.321(4)
		δ_0	-0.006(2)	-0.005(2)
		γ_V	2.529(5)	2.534(1)
		δ_V	–0.0045(4)	–0.0018(6)
	Ar	γ_0	2.573(3)	2.576(1)
		γ_2	0.283(3)	0.286(10)
		δ_0	–0.0032(3)	–0.0019(9)

2.3 Resonator spectrometer

This spectrometer was used for recordings of the R(0) and R(1) lines in pure CO at pressures of 200, 250, and 300 Torr and in CO–Ar mixtures at pressures up to 1500 Torr. The relative fraction of CO in a mixture varied within 3–14 % and 0.7–14 % for the R(0) and R(1) line recordings, correspondingly. Experimental conditions are given in Table 5. The plus and minus symbols in the table indicate that the corresponding spectrum was or was not registered, respectively.

All spectra were obtained at a temperature of 297.1±0.6 K. For each gas mixture, several spectra were recorded, corresponding to different distances between the quasioptical-waveguide system and the resonator. Averaging of these spectra allowed decreasing the impact of the parasitic reflections of radiation in the spectrometer waveguide on the experimental results (see details in Koshelev et al.[50]). The spectra were analyzed as follows. At the first step, the total contribution of other lines (except the investigated R(0) or R(1) lines) calculated for the experimental conditions was subtracted from each recording. Each line in this calculation was modeled by the Van Vleck — Weisskopf profile supplemented by the first-order line mixing term (VVWLM profile also known as Rosenkranz profile[51]):

$$f_j^{VVWLM}(\nu) = \frac{I_j}{\pi}\left(\frac{\nu}{\nu_0^j}\right)^2\left(f_j^p(\nu-\nu_0^j)+f_j^n(\nu+\nu_0^j)\right) \qquad (6)$$

$$f_j^p(\nu) = \frac{\Gamma_j + Y_j(\nu)}{\Gamma_j^2+\nu^2}, \quad f_j^n(\nu) = \frac{\Gamma_j - Y_j(\nu)}{\Gamma_j^2+\nu^2}, \qquad (7)$$

where $I_j, \nu_0^j, \Gamma_j, Y_j$ are integrated intensities, central frequencies, half-widths, and first-order line mixing parameters, respectively, for the j-th line in the spectrum.

The far wings of the profile were truncated at 25 cm^{-1} detuning from its maximum to exclude uncertain influence of the line wings beyond the validity limits of the impact approximation. The cut-off frequency value of 25 cm^{-1} was chosen empirically for modeling the water vapor spectrum in the Earth's atmosphere[3]. This value appears somewhat overestimated, as discussed in Serov et al.[16]. However, we use it for modeling as an upper limit of the cut-off frequency.

Such a profile has a break (absorption step) at frequency detuning equal to the cut-off frequency. To avoid this, the absorption coefficient is commonly reduced by an almost constant value

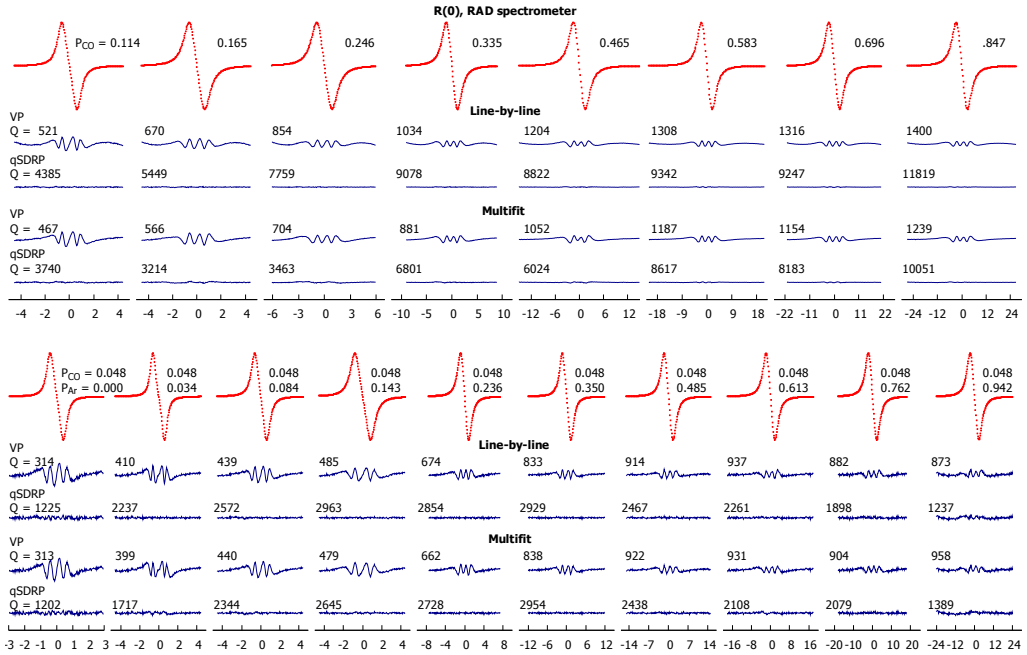

Fig. 4 Same as Fig. 1, but for the RAD spectrometer.

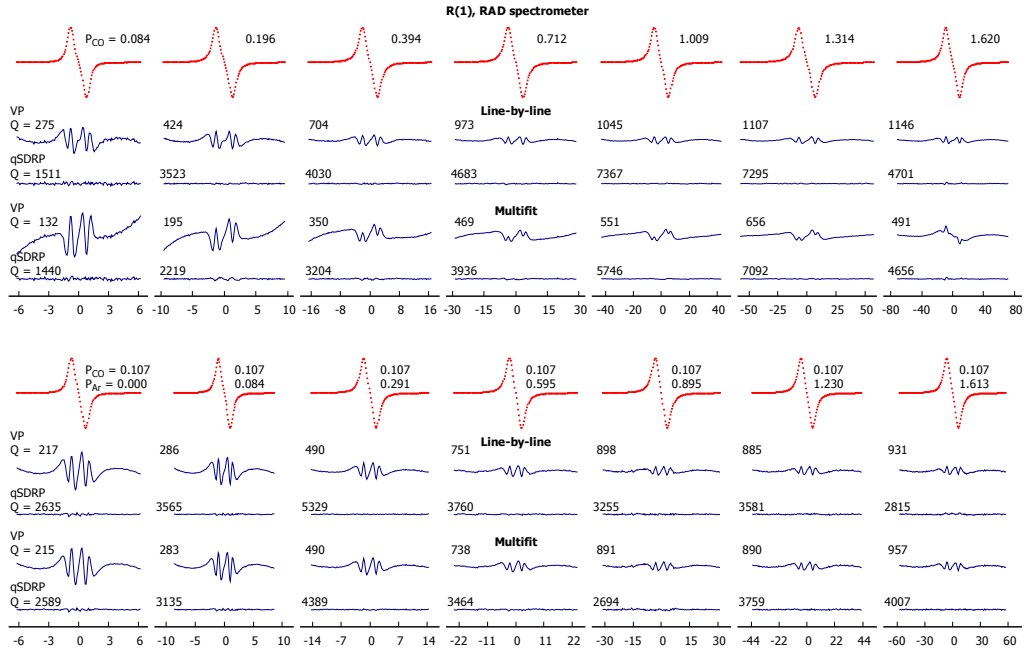

Fig. 5 Same as Fig. 4, but for the R(1) line.

Table 5 Conditions for the resonator spectrometer recordings. Plus symbol means that the recording has been made.

No	P_{CO}, Torr	P_{Ar}, Torr	R(0)	R(1)
1	5	748	—	+
2	10	745	—	+
3	10	999	—	+
4	10	1240	—	+
5	10	1493	—	+
6	25	748	+	+
7	25	997	—	+
8	50	748	+	+*
9	75	748	+	—
10	125	749	+	+**
11	125	996	+	+**
12	125	1120	+	+**
13	125	1245	+	—
14	125	1370	—	+**
15	125	1399	+	—
16	200	0	+**	+**
17	250	0	+**	+**
18	300	0	+**	+**

* noisy line center
** except line center

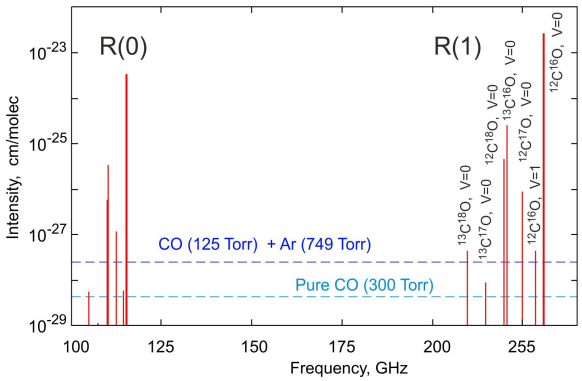

Fig. 6 Stick-diagram of the CO spectrum in the range under study in accordance with the HITRAN2020 database. The horizontal lines are for the resonator spectrometer sensitivity limit (4×10^{-9} cm^{-1}) for two most unfavorable cases (maximal absorption at the line center) of recordings in pure gas and in CO-Ar mixture. Identification is given for the R(1) lines only because the spectrum pattern is the same for both transitions.

equal to the absorption in the wing of the line at the cutoff frequency[3]. This lowering ("removing the pedestal") of the line leads to a slight change of its integrated intensity because the area under the profile is no longer equal to unity. In our work we do not make such reduction to avoid integrated intensity change. Furthermore, in our case the aforementioned steps do not exceed the experimental noise level.

Half-widths and line mixing parameters are calculated assuming binary interactions of molecules from

$$\Gamma_j = \gamma_j^{CO-CO}\cdot P_{CO} + \gamma_j^{CO-Ar}\cdot P_{Ar} \quad (8)$$

$$Y_j = y_j^{CO-CO}\cdot P_{CO} + y_j^{CO-Ar}\cdot P_{Ar} \quad (9)$$

where γ_j^{CO-CO} and γ_j^{CO-Ar} are self- and argon-broadening coefficients, y_j^{CO-CO} and y_j^{CO-Ar} are first-order (in pressure) mixing coefficients, and P_{CO} and P_{Ar} are partial pressures. Collisional pressure shifts were omitted in the model because their influence on the result of the modeling can be safely supposed to be negligible.

The integrated intensities of the lines are proportional to the number density of CO molecules:

$$I_j = S_j(T)\cdot n_{CO} = S_j(T)\cdot\frac{P_{CO}}{k_B T}, \quad (10)$$

where S_j(T) are normalized line intensities, as supplied by spectroscopic databases.

The number density was calculated using an ideal gas approximation. It was verified in Paper I[30] that accounting for non-ideality of gas leads to number density correction, which does not exceed 0.1 % for the experimental conditions of the resonator spectrometer and thus can be safely neglected.

Intensities, central frequencies and self-broadening coefficients were taken from the HITRAN2020 database[43]. Only lines with intensities larger than 10^{-28} cm/molec were taken into account. The lines with $\nu_0 > 100$ cm^{-1} were omitted. Ar–broadening coefficients were determined according to Luo et al.[52]. The vibrational dependence of the broadening was neglected owing to the (nearly) triple bond of CO. Figure 6 presents the CO spectrum diagram in the range near the R(0) and R(1) rotational transitions. It demonstrates that notable contribution to the absorption can be from lines of the most abundant isotopologues in the ground vibrational state and rotational lines of the first excited vibrational state of the main CO isotopologue.

The J–dependence of the line mixing coefficients was determined by the iterative procedure starting with the experimental data on He–broadening of CO lines from Predoi-Cross et al.[28] At the first step, we supposed that $y_{R(J)}^{CO-CO} = y_{R(J)}^{CO-Ar} = y_{R(J)}^{CO-He}$. At the second step, after analysis of our experimental data and determination of y coefficients for the R(0) and R(1) lines, the $y_{R(J)}$ coefficients were calculated for both the self- and Ar-broadening cases as:

$$y_{R(J)} = \begin{cases} y_{R(0),exp} & \text{for } J=0, \\ y_{R(1),exp} & \text{for } J=1, \\ y_{R(J-1)}\cdot\frac{y_{R(J)}^{CO-He}}{y_{R(J-1)}^{CO-He}} & \text{for } J>1; \end{cases} \quad (11)$$

Another possibility of calculating the J-dependence is based on the $y_{R(J)}^{CO-CO}$ data provided by the HITRAN2020 database (see also Hashemi et al.[53]). For an unknown reason these coefficients are equal to zero for $J \le 3$ and values for $J > 3$ differ from the coefficients calculated using equation (11) on the basis of our experimental results (Fig. 7)

Note that the use of self-mixing coefficients from HITRAN instead of our approximation for $J > 3$ does not have a notable effect on the values of the retrieved line shape parameters (frequency, width, intensity, mixing), but will slightly impact the additive term responsible for the continuum (which is detailed below). This effect is small and close to the sensitivity limit of the spectrometer.

A more detailed analysis of how the uncertainties of line shape

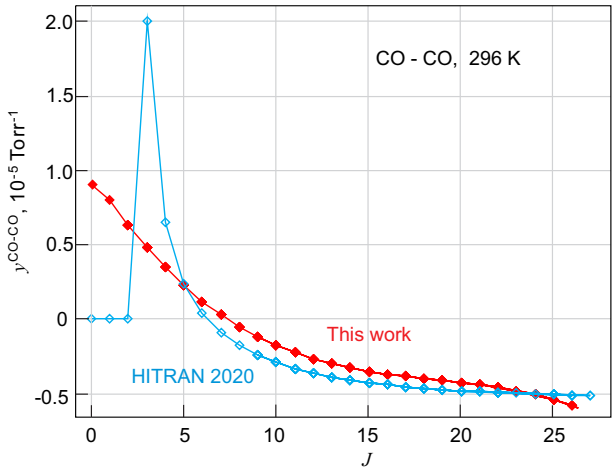

Fig. 7 CO–CO first-order line mixing coefficients versus quantum number J in rotational band. Red diamonds correspond to the dependence obtained using equation (11) on the basis of our experimental results (first two points) and data from Predoi-Cross et al.[28]. Blue diamonds are from the HITRAN2020 database.

coefficients of other lines of the CO spectrum can affect the retrieved coefficients of the R(0) and R(1) lines is given in Section 3.

Spectra recordings obtained at close, but slightly different conditions (e.g., Ar pressure differs by several torrs, or temperature by several tenths of kelvins) were corrected to provide their correspondence to the same conditions. The correction was calculated using formulae (6-7) for the total spectrum modeling. After the correction, the spectra were averaged. Thus, we obtain a number of averaged spectra, each of which corresponds to specific conditions (P_{CO} and P_{Ar}).

The averaged spectra were fitted by the speed-dependent Van Vleck — Weisskopf model, which accounts for SD of collisional cross-section and line mixing effect (SDVVWLM). In a general form (see the speed-dependent line shape analog proposed by Pickett[54]) this resonance line shape model is written as:

$$F_r(\nu) = \frac{1}{\pi}\left(\frac{\nu}{\nu_0}\right)^2 \int_0^\infty \left(\frac{\Gamma(z)+Y(z)(\nu-\nu_0-\Delta(z))}{\Gamma(z)^2+(\nu-\nu_0-\Delta(z))^2} + \frac{\Gamma(z)-Y(z)(\nu+\nu_0+\Delta(z))}{\Gamma(z)^2+(\nu+\nu_0+\Delta(z))^2}\right) f_{MB}(z)dz, \quad (12)$$

where $z = \upsilon/\upsilon_m$ is a reduced speed, with υ and υ_m being the active molecule speed and its most probable speed, respectively.

The quadratic approximation of the speed-dependence of line shape parameters was adopted as recommended by IUPAC[55]:

$$X(z) = X_0 + X_2\left(z^2 - \frac{3}{2}\right), \quad (13)$$

where X is either Γ,Δ or Y. Taking this into account, the general line shape profile (12) reduces to the qSDVVWLM profile. The latter can be reduced to the qSDVVW profile by letting $Y_{0,2} = 0$ and to the VVWLM profile with $\Gamma_2 = \Delta_2 = Y_2 = 0$. To reduce the number of variable parameters we neglected the speed-dependence of the line mixing parameter Y, because its impact was found to be much less than the experimental noise level for the R(0) line[30]. Additional theoretical calculations for both lines confirm this fact (Section 4). For fitting the experimental spectra, the general profile should be multiplied by the integrated intensity I of the line and complemented by an additional "pedestal" function $F_c(\nu)$ responsible for the continuum absorption in pure CO or CO–Ar mixtures. Thus, the model for the spectra fitting is

$$F(\nu) = I \cdot F_r(\nu) + F_c(\nu). \quad (14)$$

Frequency dependence of the continuum was approximated by the quadratic polynomial:

$$F_c(\nu) = C_0 + C_2\nu^2. \quad (15)$$

Such a behavior of the continuum in the millimeter-wave range was demonstrated for many molecular systems (e.g., H_2O–N_2[56], N_2–N_2[57], CO_2–CO_2 and CO_2–Ar[58]). This quadratic growth is a general property of matter stipulated by the frequency dependence of the so-called radiation term (see, e.g., Frommhold[4]). The constant C_0 does not have a strict physical meaning. It may take into account minor deviation of the continuum from the ν^2 dependence. In practice it corresponds to small systematic apparatus effects which impact the shape and the absolute value of the pedestal.

As an example of using the model (14), Fig. 8 demonstrates the manifestation of both SD and line mixing effects for the averaged spectrum corresponding to P_{CO} = 125 Torr and P_{Ar} = 753 Torr. Characteristic systematic deviations are seen in the fit residuals if the model does not take one or another effect into account. Maximal fit quality reaches 2600 for the qSDVVWLM model, which corresponds to the SNR of this experimental spectrum.

The R(1) line intensity is approximately 8 times higher than the intensity of the R(0) line. Therefore, all other things being equal, the absorption coefficient in the maximum of these lines will have the same proportion. For CO partial pressures above about 50 Torr, the resonator response signal near the maximum of the R(1) line becomes too broad and, therefore, too weak to be reliably measured. These frequency points near the line maximum were omitted for such spectra. The corresponding spectra (Table 5, Nos. 10, 11, 12 and 14) were treated using the qSDVVWLM profile with fixed parameters ν_0, $\Delta_2 = Y_2 = 0$ and Γ_2. The latter was taken from RAD results (Table 4).

The spectra of pure CO were analyzed in a slightly different way. The resonator response signal was too weak near the line maximum due to strong absorption. Thus, the line wings were recorded only. A typical example is given in Fig. 9. It shows that absorption cannot be measured in the range near the line center. The maximum measurable (in the current version of the spectrometer) absorption coefficient is about 5×10^{-5} cm^{-1}, which is smaller than the absorption around the line maximum. Most parameters of the qSDVVWLM profile are fixed: (i) intensities are taken from HITRAN2020 database; (ii) central frequencies are from Lamb-dip measurements[22]; (iii) the broadening coefficients are taken from the RAD spectrometer data (Table 4). The gas pressure, Y parameter and parameters of the pedestal C_0 and C_2 are free parameters of the model. The deviation of CO pressure determined from the fit from Baratron gauge readings is within 0.4 %, which exceeds the declared uncertainty of the

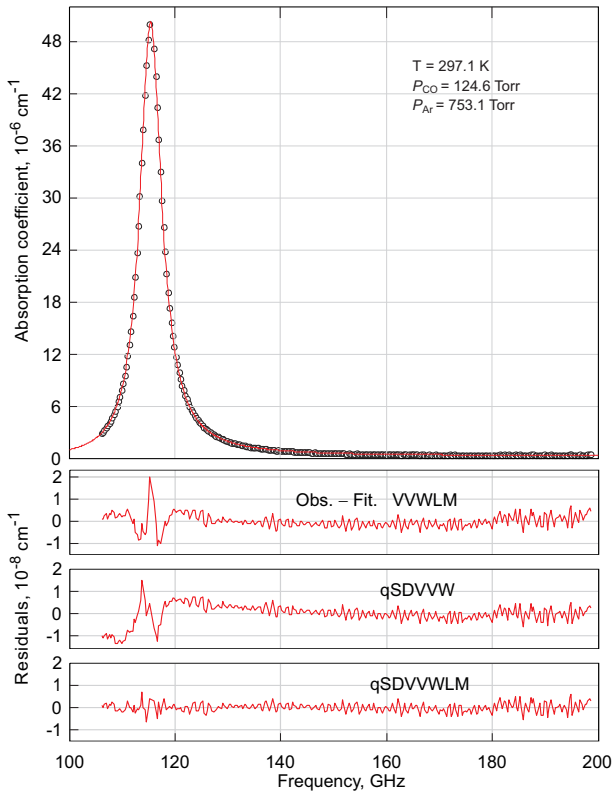

Fig. 8 Upper panel: experimental spectrum of a CO-Ar mixture in the R(0) line region (points) and its approximation (solid curve) using Eq. (14); lower panels: residuals of the approximation for VVWLM, qSDVVW and qSDVVWLM line profiles.

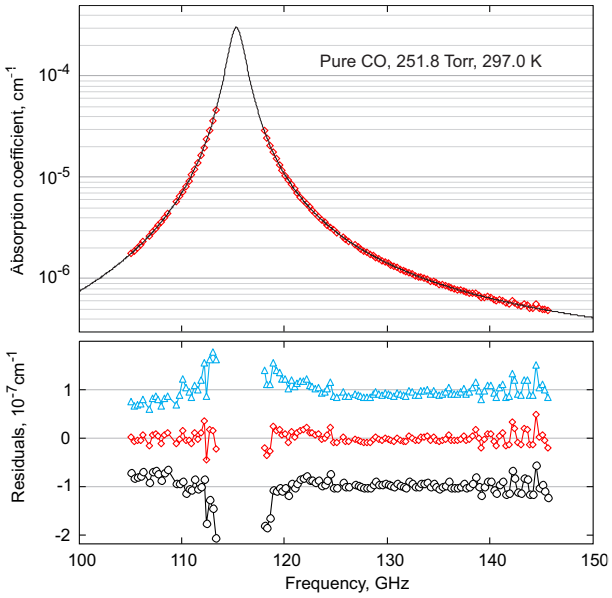

Fig. 9 Upper panel: Measured absorption in pure CO (diamonds) and model (14) with the VVWLM profile, fitted to experimental points (line); lower panel: residuals for three fixed values of CO pressure, used in the model: $P = P_0 = 252.78$ Torr (red diamonds), $P = 1.0015P_0$ (black circles), and $P = 0.9985P_0$ (blue triangles). The two latter residuals are shifted up and down by 10^{-7} cm^{-1} for clarity.

gauge (0.25 %). This deviation can be explained by the inaccuracy of the line integrated intensity in the HITRAN database, which will be discussed below (Section 3). We emphasize that even a small change of CO partial pressure of about 0.1 %, leads to a significant change of the residual (Fig. 9). This demonstrates that our resonator spectrometer can be used for calibration of pressure gauges (if the intensity and the self-broadening parameter of a line are known with sufficiently low uncertainty).

An example of the combined spectra of the R(0) and R(1) lines is shown in Fig. 10. Note the remarkable agreement of the spectra in the range of their overlapping (near 150 GHz) despite the different spectrometer configurations used for their recording (different radiation sources, different elements of a waveguide line, including attenuator, horns, etc.). This plot also demonstrates a smooth continual pedestal $F_c(\nu)$, determined from the fit of the model (Eq. (14)) to experimental points. The latter corresponds to the retrieved continuum, commonly determined as the difference of the measured absorption coefficient and the total calculated contribution of the resonance lines. Figure 10 shows that the continuum significantly exceeds the spectrometer sensitivity limit and can be extracted with sufficient accuracy. The contribution of the continuum reaches 20 % of the total absorption near the local minimum, i.e. the gas transparency microwindow, between the lines, which implies that it should not be neglected in the absorption model. More detailed analysis of the continuum component and its physical nature is beyond the scope of the present paper and will be presented in our future publications.

After retrieving parameters of the observed lines, the line shape coefficients are determined from the fit of the following linear function to experimental points

$$\frac{X}{P_{CO}} = x^{CO-CO} + x^{CO-Ar}\frac{P_{Ar}}{P_{CO}}, \qquad (16)$$

where x is either γ_0, γ_2 or y ($x_{0,2} = X_{0,2}/P$). The results are shown in Fig. 11. The coefficients γ_0^{CO-CO} and γ_0^{CO-Ar} are determined with low uncertainty for both lines. The relative uncertainties of γ_2 coefficients are significantly higher. In particular, for the R(1) line the relative uncertainty of γ_2^{CO-CO} coefficient is 56 %, and the obtained value of 2.3(13) MHz/Torr diverges from the corresponding value obtained from RAD spectrometer data by an order of magnitude. So we decided to fix the γ_2^{CO-CO} coefficient for this line to the value obtained from RAD spectrometer data (Table 3), and retrieved only the γ_2^{CO-Ar} coefficient. Note, that the obtained value of $\gamma_2^{CO-Ar} = 0.283(16)$ MHz/Torr (if γ_2^{CO-CO} coefficient is fixed) is in agreement within statistical uncertainty with the initial value of 0.236(32) MHz/Torr (if γ_2^{CO-CO} is a free parameter). Line mixing coefficients y^{CO-CO} and y^{CO-Ar} are confidently retrieved for both R(0) and R(1) lines. To the best of our knowledge, this is the first measurement of mixing coefficients for other than oxygen fine structure lines in the millimeter- and submillimeter-wave range.

The speed-dependent shifting parameter Δ_2 is very small (as follows from our *ab initio* calculations, Fig. 3 from Paper I[30]) for

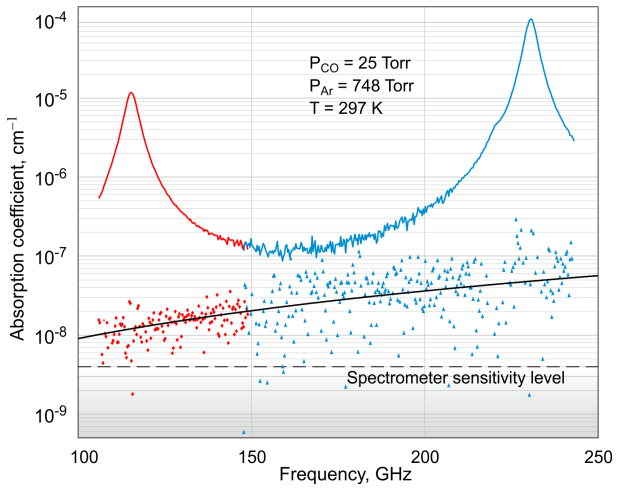

Fig. 10 The combined spectrum of two experimental recordings of CO-Ar gas mixture (red and blue lines). Red diamonds and blue triangles show the retrieved continuum (see the text for details). Black solid line corresponds to the continual pedestal, obtained from the model fit. Dashed line - the sensitivity level of the spectrometer.

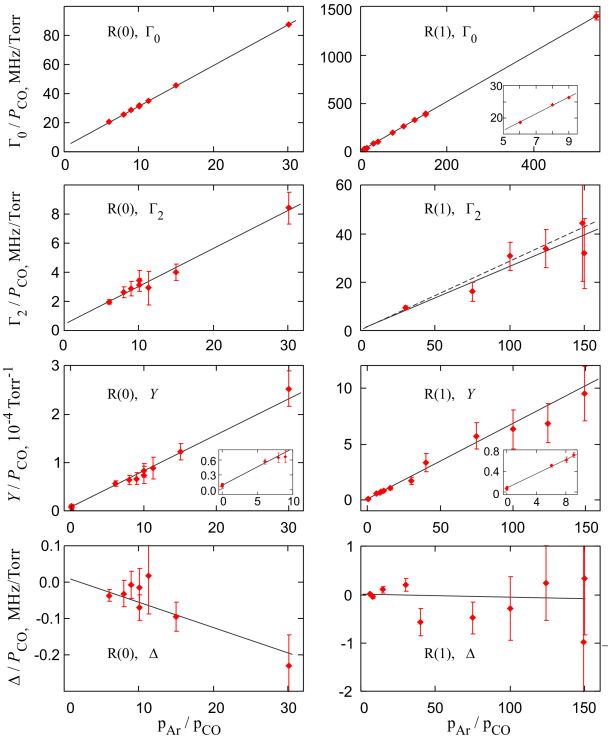

Fig. 11 Line shape parameters for the R(0) (left column) and R(1) (right) lines versus the ratio of Ar and CO partial pressures. Experimental values are shown by diamonds. Error bars correspond to $\pm 3\sigma$ statistical uncertainty. Straight lines correspond to Eq. (16) fitted to points (weight of point is σ^{-2}). Dashed line — fit with fixed $\gamma_2^{CO-CO} = 0.321$ MHz/Torr (see the text for details). The inserts show a zoomed area near the coordinate origin.

the lines under study and could not be reliably retrieved at the current sensitivity level of the spectrometer. Therefore, we set $\Delta_2 = 0$ in the model and only Δ_0 was varied. Still, the self-shifting coefficient cannot be reliably retrieved from these spectra. In pure CO they do not include the central part of the line (Fig. 9) and CO-Ar spectra are recorded with low partial pressure of CO. Overall the pressure shifting effect in gases under study is very small and comparable with the measurement uncertainty. The scarce data on line shifting retrieved from the resonator spectrometer spectra will be discussed together with the related RAD spectrometer results in the next section.

Measured intensities of the R(0) and R(1) lines at various partial pressures of CO are shown in Fig. 12.

The multifit procedure was also used for the analysis of the resonator spectrometer recordings, with expected dependences of collisional parameters on P_{CO} and P_{Ar}. Two approaches were tested regarding fitting the integrated intensity I. In one of them, the intensity was fitted for each recording, in the other one, it was a joint (variable) parameter for all spectra. Both methods gave similar results but the former was found to be more robust. The continuum absorption term was modeled as follows

$$F_c(\nu) = C_0 + C_2^f \nu^2 P_{CO} P_{Ar} + C_2^s \nu^2 P_{CO}^2, \qquad (17)$$

where C_2^f and C_2^s are variable parameters responsible for the foreign- and self-continuum components in CO-Ar mixtures. The C_0 parameter is free for each recording.

Figure 13 presents results of line-by-line and multispectrum fitting for resonator recordings of the R(0) and R(1) lines in CO–Ar mixtures. The collisional parameters obtained with these two different methods are given in Table 6.

3 Analysis of uncertainties

First of all we note that most line shape coefficients retrieved from experimental spectra by both our methods agree within statistical uncertainty for all three instruments (Tables 2, 4, 6). The agreement within 1σ is achieved for 85, 79 and 75 % of parameters obtained from recordings by the RAD, resonator and video spectrometer, respectively. Only for two poorly determined coefficients ($\gamma_{2,R0}^{CO-CO}$ from video data and $\gamma_{2,R1}^{CO-Ar}$ from resonator data) the deviation is near 3σ.

The final set of experimentally determined line shape coefficients is obtained from analysis of the data from all three instruments. Weighted averaging is used in most cases. The result is shown in Table 7 together with *ab initio* data, and available data from other sources.

Note that all the retrieved parameters are recalculated to 296 K using the ordinary power law. The value of the temperature exponent $n_\gamma = 0.78$ obtained from *ab initio* calculations (Section 4) is used for both lines. For simplicity, the same exponent value is used for recalculation of all other collisional line shape parameters. Since the temperature variations are small (the correction does not exceed 1 % of the parameter value in most unfavorable cases), the potential inaccuracy of the exponent value results in much smaller changes and thus can be neglected in the total error budget.

The total uncertainty of each parameter was calculated as:

$$\begin{aligned} \delta X_{sum} &= X\sqrt{\left(\frac{\delta X_{fit}}{X}\right)^2 + \left(\frac{\delta P}{P}\right)^2 + m^2\left(\frac{\delta T}{T}\right)^2} \\ &= X\sqrt{(\varepsilon_{fit})^2 + (\varepsilon_P)^2 + m^2(\varepsilon_T)^2}, \end{aligned} \qquad (18)$$

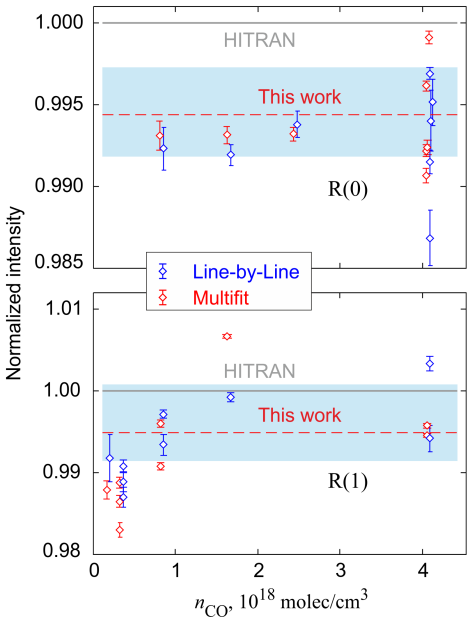

Fig. 12 Measured and re-scaled to 296 K intensities of the R(0) and R(1) lines (points) with statistical uncertainties ($\pm 3\sigma$). Blue points in both graphs are shifted to the right by 0.04 units for clarity. Blue areas correspond to the weight averaged result for blue points. Dashed lines are for the final values determined from this work on the basis of the multifit procedure. All data are normalized by the corresponding values from the HITRAN2020 database (Table 7).

where m is the temperature-dependence exponent for the parameter X (e.g., in the case of broadening parameter $m = 0.78$ and in the case of line intensity $m = 1$), $\varepsilon_P = 0.002$ is relative pressure uncertainty, $\varepsilon_T \approx 0.1/297 = 0.0003$ is relative temperature uncertainty.

The impact of the analytical modeling of the baseline as a polynomial is evaluated for RAD and video spectrometers. Coefficients of the polynomial and retrieved line shape parameters are correlated. The higher the degree of the polynomial, the larger the potential systematic error of the parameters. It was found, however, that the impact of changing the order of the polynomial (up to the third order) is less than the statistical uncertainty of the retrieved parameters.

The final uncertainty of experimentally determined coefficients (shown in parentheses in Table 7) also includes our assessment of the uncertainty associated with the systematic effects identified in this study and discussed below in the corresponding subsections.

One of uncertainty sources for *ab initio* data is the intermolecular interaction potential used for data calculations. In Paper 1, in order to calculate the parameters of the R(0) line, the Sumiyoshi and Endo potential[35], as well as the more recent Cybulski potential[36] were used. Relative deviation between two sets of these data allows evaluating the potential-related uncertainty of line shape collisional coefficients. For γ_0, γ_2 and δ_0 at room temperature, the deviation is about 1.8, 5 and 21 %, correspondingly. These uncertainties are given for *ab initio* data in Table 7. It is worth noting that γ_0^{Sum}=2.794 MHz/Torr, and γ_2^{Sum}=0.264 MHz/Torr theoretically calculated for the R(0) line

Table 6 Line shape coefficients for the R(0) and R(1) lines at 296 K from the resonator spectrometer recordings: broadening and shifting coefficients are given in MHz/Torr, mixing coefficients in 10^{-6}/Torr, and intensity in 10^{-24}cm/molec. One standard deviation of the parameter value obtained from the fit is given in parenthesis.

Line	Gas	Coef.	Line-by-line	Multifit
R(0)		I	3.2816(34)	3.2814(32)
		γ_W	3.54(6)	—*
		y	9.4(14)	8.3(4)
		δ	0.02(2)	–0.004(2)
	CO	γ_0	3.56(4)	—*
		γ_2	0.42(14)	—*
		y_0	8.3(10)	7.6(3)
		δ_0	0.015(20)	–0.009(2)
		γ_W	2.743(6)	2.749(2)
		y	8.7(3)	8.45(25)
		δ	–0.008(1)	–0.004(2)
	Ar	γ_0	2.792(5)	2.798(2)
		γ_2	0.261(16)	0.288(7)
		y_0	7.45(23)	7.16(24)
		δ_0	–0.006(2)	–0.003(2)
R(1)		I	25.56(4)	25.53(6)
		γ	3.55(13)	—*
		y	7.8(9)	6.86(15)
		δ	0.001(40)	0.004(2)
	CO	γ_0	3.10(11)	—*
		γ_2	—*	—*
		y_0	7.9(10)	6.7(2)
		δ_0	–0.006(40)	0.005(3)
		γ	2.537(11)	2.5380(9)
		y	6.83(14)	7.41(18)
		δ	–0.006(21)	–0.005(1)
	Ar	γ_0	2.591(9)	2.567(3)
		γ_2	0.286(16)	0.214(5)
		y_0	6.73(16)	6.95(20)
		δ_0	0.009(21)	–0.005(1)

* Fixed to the value from Table 7

using the Sumiyoshi and Endo potential are in remarkable agreement with experimentally determined values within their uncertainty. Similar data derived from the use of the Cybulski potential have a larger deviation (Table 7). For the R(1) line only calculations with the Cybulski potential have been carried out. They demonstrate a relative deviation from experimental values similar to the R(0) line. For the coefficient γ_0, the deviation exceeds the measurement uncertainty for both lines.

3.1 Broadening

Comparison of collisional broadening parameters obtained from different spectrometers (Tables 2, 3, 6) reveals that in most cases the corresponding values agree with each other within their statistical uncertainties. There are a few exceptions indicating the existence of systematic effects. One of the most probable reasons is the aforementioned impact of the instrumental baseline through correlation of the model parameters. Another potential reason of discrepancies in foreign gas broadening measurements (Ar-broadening, in particular) is an uncontrolled partial pressure of CO when Ar is gradually added into the gas cell. The variation

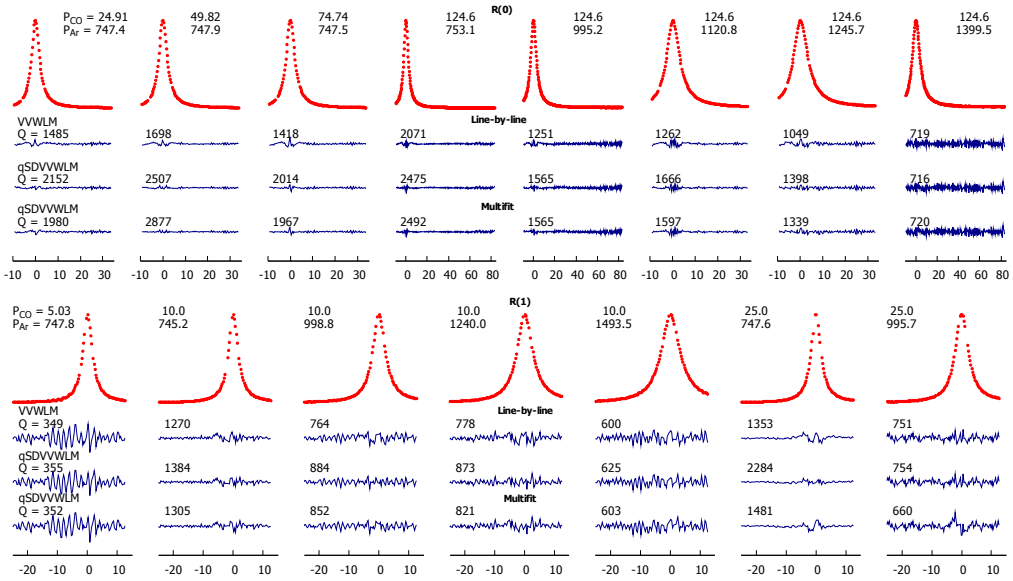

Fig. 13 Residuals (solid traces) of line-by-line and multispectrum fits of the VVWLM and qSDVVWLM models for the R(0) (upper panel) and R(1) (lower panel) lines recorded using the resonator spectrometer (points). Partial pressures of CO and Ar and fit quality factors Q are indicated near the recordings.

of CO content can be due to remaining disequilibrium conditions and/or adsorption/desorption processes in a gas cell and related vacuum system. Nevertheless, we can assert that the presence of the systematic errors and their impact on the final value is significantly reduced if data from all three instruments are analyzed together. This is demonstrated on the example of the joint dependence of broadening parameters versus argon pressure covering the enormous, for spectroscopic studies, pressure range from 2×10^{-2} to 1.4×10^{3} Torr, which is shown in Fig. 14 for both lines after subtraction of the self-broadening contribution. A standard deviation of the points corresponding to γ_V for the R(0) line is 23 kHz/Torr, which is near 1 % of the broadening parameter value.

The lower panels of Fig. 14 present a similar deviation for Γ_0^{CO-Ar} points obtained from the same experimental data set. It clearly reveals the problem of correlation between the parameters in the line shape model. The more parameters are included in the model, the larger the systematic deviation of the retrieved line shape parameters. Systematic overestimation of the broadening parameters Γ_V^{CO-Ar}, Γ_0^{CO-Ar} and Γ_2^{CO-Ar} for the R(1) line is notable for the video spectrometer data. The value of the systematic error is, however, comparable to the deviation from one experimental series to another, evidencing that its origin is in the baseline instability related to temperature drift during spectra recordings. Taking this into account, we did not use these data for the final parameter values determination.

3.2 Shifting

The pressure shifting effect is very weak for the lines under study in both CO–CO and CO–Ar collisional systems. Analysis of the video spectrometer data reveals that the baseline related systematic uncertainty of line center measurements is about ±10 kHz (note that statistical error is smaller by about an order of magnitude), which makes small shifts immeasurable with this instrument. The RAD spectrometer data also show a significant scattering of experimental points, which makes self- and Ar-shifting data indistinguishable (Fig. 15, left panels). The spread of points increases with an increase in pressure. Nevertheless, the sign and approximate value of the effect can be evaluated as $-4(2)$ and $-3(2)$ kHz/Torr for the R(0) and R(1) lines, respectively. Note that the unshifted ("zero-pressure") positions of lines averaged over all these series are 115 271 202 .08(22) and 230 538 000.32(32) kHz in a perfect agreement with the frequencies of these transitions from Winnewisser et al.[22].

To compare the results retrieved from the analysis of the RAD and the resonator spectrometer data, we normalized the observed shift of the R(0) and R(1) lines from the aforementioned unshifted positions by the total gas pressure. The result is shown in the right panel of Fig. 15. The figure demonstrates that data obtained from both instruments agree with each other and with results of *ab initio* calculations (Table 7).

3.3 Mixing

One can notice some difference between the values of the mixing coefficients y and y_0 retrieved using speed-independent (SI) and speed-dependent (SD) profiles, respectively, for the R(0) line (Table 6). The use of the SI-profile under the conditions when the SD-related features are well observed leads to the systematic difference of the retrieved profile parameters. This phenomenon manifests itself stronger for minor effects, which was confirmed by the numerical experiment. For the R(1) line the difference is not so pronounced, as the SNR of the corresponding recordings is smaller than for the R(0) line.

The experimental values for the (first order in pressure) line mixing coefficients are about 9 % and 18 % larger than the results of *ab initio* calculations for the R(0) and R(1) line, respectively

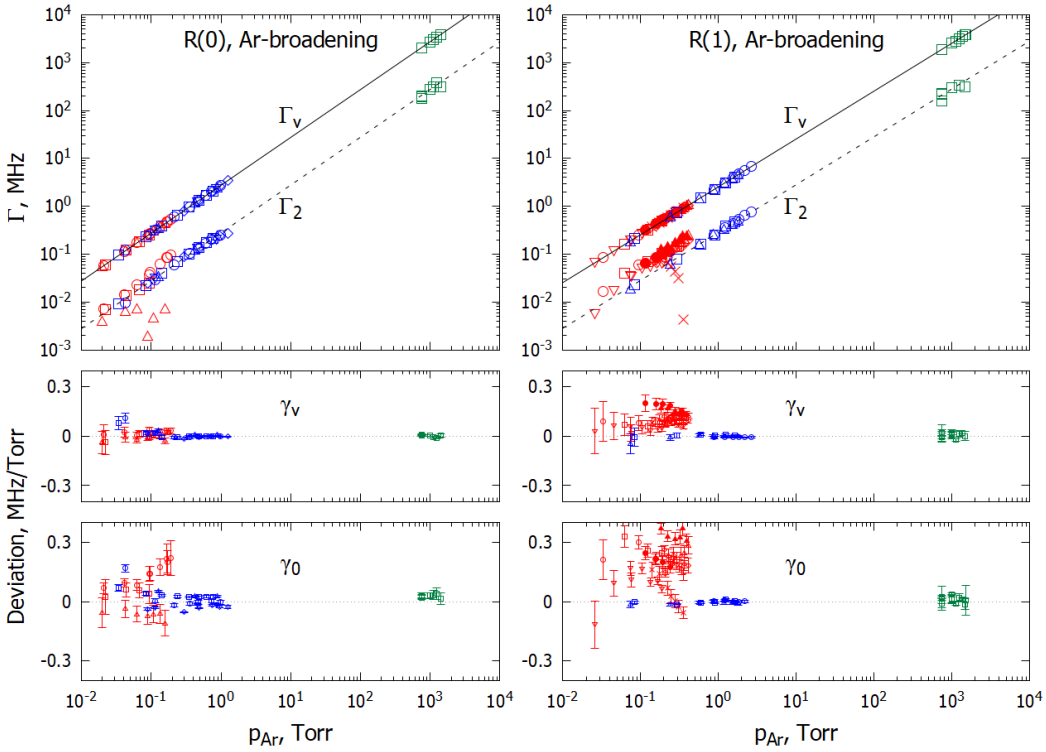

Fig. 14 Joint dependence of retrieved Γ_V^{CO-Ar} and Γ_2^{CO-Ar} parameters versus Ar pressure (upper panel). The difference between experimental data normalized by Ar pressure and the average value of γ_V^{CO-Ar} (middle panel). The same as middle panel but for Γ_0^{CO-Ar} (lower panel). Red, blue and green symbols are for the video- , RAD- and resonator-spectrometer, respectively. Circles, triangles and squares of the same color are for different experimental series. Error bars correspond to 3σ statistical uncertainty.

Table 7 Experimental and theoretical results from this work and related previous data. Broadening and shifting coefficients are in MHz/Torr, mixing coefficients in 10^{-6}/Torr and intensity in 10^{-24} cm/molec

Line	Gas	Coeff.	Avg.exp.	*Ab initio*[a]	HITRAN	Other
R(0)		I	3.2814(73)	—	3.300[d]	—
	CO	γ_V	3.419(13)	—	3.432[g]	3.499(3)[b]
		γ_0	3.472(14)	—	3.471[g]	3.546(9)[b]
		γ_2	0.32(2)	—	0.367[i]	0.30(3)[b]
		δ_0	–0.004(2)	—	–0.013[j]	—
		y_0	8.0(5)	—	—	—
	Ar	γ_V	2.740(14)	—	—	2.756(2)[c]
		γ_0	2.789(14)	2.7506(1)[e](481)[f]	—	—
		γ_2	0.280(14)	0.2572(3)[e](122)[f]	—	—
		δ_0	–0.004(2)	–0.0042(4)[e](9)[f]	—	—
		y_0	7.3(5)	6.63(50)[e,h]	—	—
R(1)		I	25.53(13)	—	25.66[d]	—
	CO	γ_V	3.290(13)	—	3.195[g]	3.351(2)[b]
		γ_0	3.375(14)	—	3.235[g]	3.412(6)[b]
		γ_2	0.313(16)	—	0.343[i]	0.37(2)[b]
		δ_0	–0.003(2)	—	–0.008[j]	—
		y_0	7.3(5)	—	—	—
	Ar	γ_V	2.536(13)	—	—	2.532(2)[c]
		γ_0	2.575(13)	2.5287(1)[e]	—	—
		γ_2	0.278(16)	0.2620(3)[e]	—	—
		δ_0	–0.003(2)	–0.0037(4)[e]	—	—
		y_0	7.0(4)	5.95(50)[e,h]	—	—

[a] Cybulski potential[36], see Serov et al.[30] for details
[b] From Seleznev et al.[27]
[c] From Luo et al.[52]
[e] Statistical uncertainty of fit, see Section 4 for details
[f] Uncertainty due to the intermolecular potential, see text for details
[h] Uncertainty is roughly estimated as about 10 %
HITRAN stated uncertainties:
[d] less than 1 %
[g] 2–5 %
[i] 5–10 %
[j] more than 20 %

(Table 7). We estimate the uncertainty of calculations to be about 10 %, so we can speak about the agreement for the R(0) line but the joint experimental and theoretical uncertainty does not justify the deviation for the R(1) line. The most probable reason, in our opinion, is related to the impact approximation (slowly decaying Lorentzian wings of the lines), which was implicitly assumed in the calculations. Thus the deviation is directly linked to the observed continuum (Fig. 10) and will be discussed in detail in our future publications.

3.4 Intensity

Figure 12 presents the measured integrated intensity for both lines. Weighted averaged results from line-by-line and multifit procedures agree within standard deviation of data points. The final values (from multifit, as it is less prone to systematic errors) are slightly smaller than the HITRAN2020 data for both lines. For the R(0) line, the difference is statistically significant. The obtained value is smaller by about 0.5 %: $S_{exp}/S_{HITRAN} = 0.994(2)$ and the difference is about 3 times larger than the measurement uncertainty. For the R(1) line, the relative deviation is very similar but in this case it is comparable to the uncertainty of the experimental result: $S_{exp}/S_{HITRAN} = 0.996(4)$. Note that, in the HITRAN database, the declared intensity uncertainty for these lines is less than 1 %.

3.5 Influence of other CO lines

The uncertainty of line shape parameters for R(J), $J > 1$ lines of the CO spectrum potentially contributes to the uncertainty of the data retrieved from the resonator spectra through the subtraction of their modeled contribution to the observed spectra. To evaluate this uncertainty numerically we systematically perturb (increase or decrease) one of selected shape parameters for all lines of the CO spectrum, except for the line under study. The tested parameters include self- and Ar-pressure broadening and mixing coefficients as the ones that can most strongly influence the results of this work. A parameter perturbation value was estimated on the basis of uncertainty of this parameter for CO lines. In particular, for the variation of the self-broadening coefficient we adopted HITRAN's relative uncertainty of 10 %; for the Ar-broadening, 1 % was adopted as a conservative estimation on the

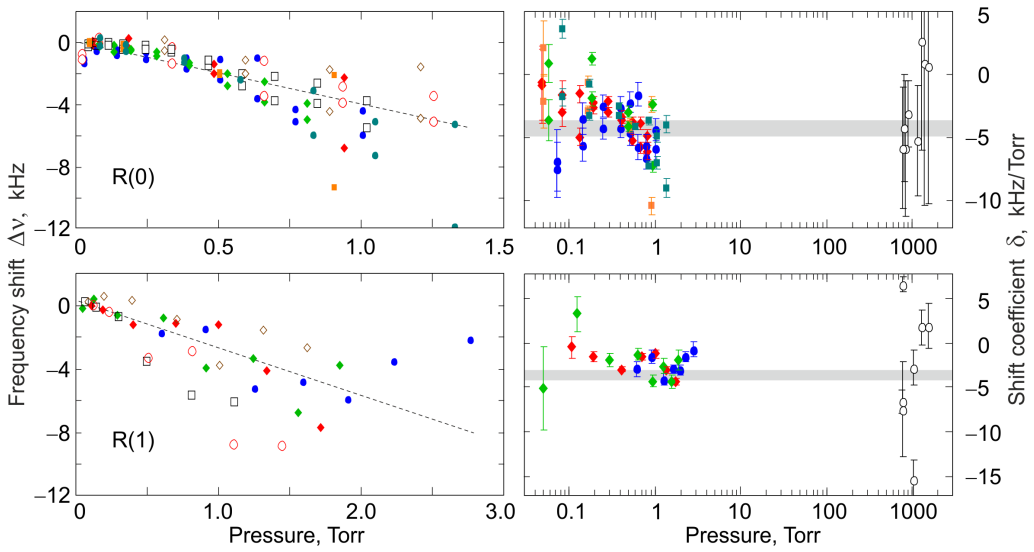

Fig. 15 Pressure shifting of the R(0) (upper panels) and R(1) (lower panels) lines. Left panels are only for RAD data in the case of self- (empty symbols) and Ar- (filled symbols) shift from 115 271 202.02 and 230 538 000.00 kHz[22]. Different symbols denote different series. Dotted lines are for average experimental values of 4(2) and 3(2) kHz/Torr for the R(0) and R(1) lines, respectively. Right panels: Pressure normalized shift from "zero-pressure" transition frequency measured by RAD (filled symbols) and resonator (empty symbols). Error bars correspond to statistical uncertainty of 1σ. Shaded areas are for results of *ab initio* calculations (Table 7). See text for details.

basis of known experimental data; for mixing coefficients in pure gas and in Ar baths, quite arbitrary relative limits of ± 30 % were chosen as the result of qualitative analysis of available data. We did not test line intensity variations because their relative impact is expected to be similar to the variation of Ar-broadening but HITRAN's uncertainty of intensity for the most influencing lines is less than 1 %. The results of this trial are presented in Table 8. Note that statistical uncertainty of the retrieved parameter does not depend on the perturbation. Its value (one standard deviation) is given in Table 8 for unperturbed parameters. The table demonstrates that the result of the perturbation does not exceed the statistical uncertainty for the majority of line shape coefficients; therefore, the corresponding error can be neglected in the total parameter uncertainty budget. As expected, the impact on the continuum coefficients is much stronger. Nevertheless, relative change of these coefficients is less than 23 %, evidencing that the observed continuum cannot be explained by uncertainty of the neighbouring line wings within the impact approximation.

4 Comparison with qualitative theoretical approaches

The observed line shape and its collisional width are determined by the average (over a very large ensemble of molecules) process of the evolution of molecular dipole between successive collisions. Within the gas kinetic theory one may define a relative speed-dependent "line width", $\Gamma(\upsilon_r)$, given by the product of molecular number density, the relative molecular speed $\upsilon_r = |\vec{\upsilon} - \vec{\upsilon}_p|$ (where υ_p is perturber speed) and an effective collisional cross-section σ, which is a function of kinetic energy $E = \mu\upsilon_r^2/2$ (where μ is the reduced mass of the collisional system). Therefore, if $\sigma(E) \propto E^q$, then the speed-dependence of the line width $\Gamma(\upsilon_r) \propto \upsilon_r{}^n$ with $n = 1+2q$ [41,54,59]. Figure 16 presents the results of *ab initio* calculations of pressure broadening cross-sections as a function of the kinetic energy for the R(0) and R(1) lines of CO highly diluted in Ar together with the straight (on a log/log scale) lines corresponding to $q = -0.28$, which is close to the value -0.25 found by Werh et al.[60] for the P(2) line of the fundamental vibrational band. The room temperature energy distribution function is also shown in Fig. 16 to give an idea about the significant range of energies.

Figure 16 demonstrates that the "power-law" approximation is quite reasonable for both lines. Standard deviation of the calculated points from the lines is near 7 Å^2 at energies within 10–1200 cm^{-1} and twice smaller for the 30–1200 cm^{-1} range. Thus, the relative speed-dependence of the line broadening parameter should be characterized by $\upsilon_r^{1+2(-0.28)} = \upsilon_r^{0.44}$.

The absolute speed-dependent broadening parameter $\Gamma(\upsilon)$ is a thermal average of $\Gamma(\upsilon_r)$ over $\vec{\upsilon}_p$, with $\vec{\upsilon}$ held constant. The conversion from $\Gamma(\upsilon_r)$ to $\Gamma(\upsilon)$ can be carried out by fitting the analytically defined function

$$\Gamma(\upsilon) = \Gamma_0(1+m_p/m)^{-n/2} M(-n/2;3/2;-(m_p/m)z^2) \qquad (19)$$

(m and m_p are masses of optically active molecule and perturber, respectively, and $M(\ldots;\ldots;\ldots)$ is the confluent hypergeometric function[54,61]) to the *ab initio* calculated data using Γ_0 as a variable parameter.

Indeed, the corresponding function with $n = 0.44$ fits well the *ab initio* data for both lines (Fig. 17). Standard deviations of the calculated points from the fitted function are 16 and 33 kHz/Torr for the R(0) and R(1) lines, respectively. Note that the deviation can be reduced down to about 10 kHz/Torr (or 0.4 % from γ_0) for both lines if n is also a variable parameter of the function (0.428

Table 8 Relative deviation in percents of the R(0) and R(1) line shape coefficients retrieved from the resonator spectrometer recordings caused by systematic simultaneous perturbation of various coefficients for all other CO lines. Zero values mean that the deviation is much smaller than the statistical uncertainty. The first lines present unperturbed values and their statistical uncertainties. Units for broadening and mixing coefficients are MHz/Torr and 10^{-6}/Torr, respectively, and for continuum coefficients 10^{-25} cm^{-1}/MHz^{2}Torr^2.

Perturbation		Retrieved coefficient					
	γ^{CO-Ar}	γ_0^{CO-Ar}	γ_2^{CO-Ar}	y^{CO-CO}	y^{CO-Ar}	C_2^s	C_2^f
R(0), unperturbed	2.749(2)	2.798(2)	0.288(7)	7.6(3)	7.16(24)	4.59(12)	5.36(4)
uncertainty, %	0.025	0.072	1.9	2.2	2.7	2.6	0.75
γ^{CO-CO} +5 %	0.0	–0.036	–1.59	0.0	–2.35	–9.1	–2.1
−5 %	0.025	0.036	0.78	1.1	1.2	7.3	1.9
γ^{CO-Ar} +1 %	–0.007	–0.072	–2.0	–	–2.4	–	-4.1
−1 %	0.033	0.072	1.2	–	2.4	–	3.9
y^{CO-CO} +30 %	0.007	0.0	–1.2	0.0	–1.2	–20	-0.94
−30 %	0.018	0.0	0.0	0.0	1.2	20	0.75
y^{CO-Ar} +30 %	–0.029	–0.11	–4.0	–	–4.7	–	–22
−30 %	0.054	0.11	3.2	–	4.7	–	22
R(1), unperturbed	2.5380(9)	2.567(3)	0.214(5)	6.7(2)	6.95(20)	4.47(17)	5.28(31)
uncertainty, %	0.031	0.078	3.6	2.4	3.8	3.8	5.9
γ^{CO-CO} +5 %	0.0	0.0	0.0	–1.5	0.0	–13.6	0.0
−5 %	0.0	0.0	0.0	1.6	0.0	13.6	0.0
γ^{CO-Ar} +1 %	0.0	0.0	0.0	—	–0.15	—	–1.7
−1 %	0.0	0.0	–0.45	—	0.15	—	1.9
y^{CO-CO} +30 %	0.0	0.0	0.0	0.40	0.0	11.6	0.0
−30 %	0.0	0.0	0.0	–0.27	0.0	–11.6	0.19
y^{CO-Ar} +30 %	0.0	0.0	0.45	—	–0.3	—	7.2
−30 %	0.0	–0.039	–0.90	—	–0.3	—	–7.0

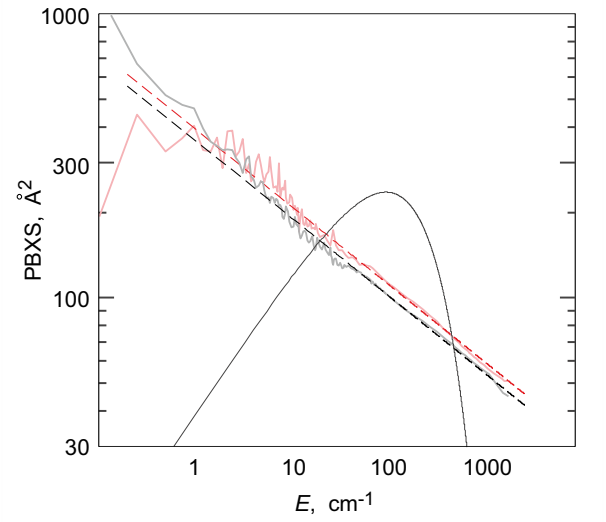

Fig. 16 *Ab initio* pressure broadening cross-sections (PBXS) versus relative kinetic energy for the R(0) (thick solid red) and R(1) (thick solid grey) lines of CO in Ar bath together with the results of approximation of these dependences above 10 cm^{-1} by the power law function $\sigma(E) \propto E^q$ for $q = -0.28$ (dashed lines). Smooth solid curve is the energy distribution function for 296 K.

and 0.469 for the R(0) and R(1) lines, respectively).

It is commonly accepted[39,55] that the speed-dependence can be approximated by the square-law formula Eq. (13). The parameters Γ_0 and Γ_2 are supposed to be derived as follows: Γ_0 is the weighed $\Gamma(\upsilon)$ with respect to the statistical weight given by the Maxwell-Boltzmann distribution $f_{MB}(z)$:

$$\Gamma_0 = \int_0^\infty f_{MB}(z)\Gamma(z)dz, \tag{20}$$

while Γ_2 value is calculated via

$$\frac{d}{dz}\gamma(z=1) = \frac{d}{dz}(\Gamma_0 + \Gamma_2(z^2 - 1.5))|_{z=1}, \tag{21}$$

that is $\Gamma_2 = 0.5\frac{d}{dz}(\Gamma(z=1))$.

This approximation is shown in Fig. 17 by the dotted curve. Note that this way of determining Γ_0 and Γ_2 coefficients from theoretically calculated speed-dependence of broadening is not unique. As an alternative, Eq. (13) can be fitted to the numerical data on $\Gamma(z)$ using $f_{MB}(z)$ as weight, either using Γ_0 as a second free parameter or fixing it to the value obtained from Eq. (20)[62,63]. The resulting Γ_0 and Γ_2 will be slightly different and in all cases the approximation notably deviates from the *ab initio* data and demonstrates worse fitting than the confluent hypergeometric function. It is therefore interesting to verify the impact of this deviation on the line shape.

The impact can be demonstrated as follows. The *ab initio* SD of collisional coefficients $\Gamma(z)$, $\Delta(z)$ and $Y(z)$ within the considered range of z can be approximated with high accuracy by a polynomial function and used for numerical calculation of the line profile using a general expression for the line profile with SD pa-

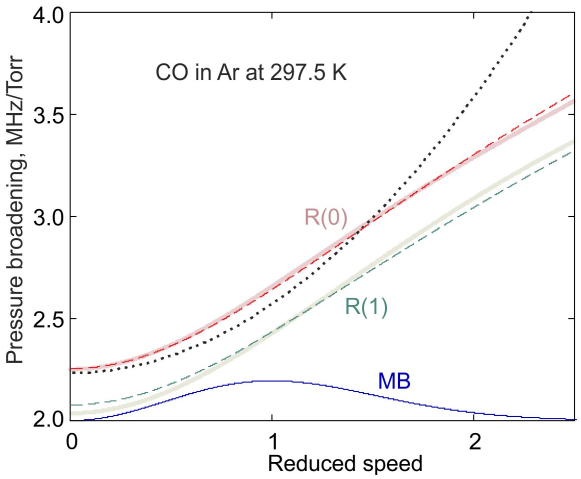

Fig. 17 Speed-dependence of collisional broadening for CO lines by Ar at 297.5 K. Thick solid red and green lines are *ab initio* data for the R(0) and R(1) lines, respectively. The result of their approximation by the quadratic function Eq. (13) for the R(0) line is shown by dotted line. Dashed lines present the result of approximation of the *ab initio* data line by the confluent hypergeometric functions with exponent value of $n = 0.44$. The lowest solid curve is the Maxwell-Boltzmann (MB) distribution of speeds. X axis is the speed of CO molecules normalized by their most probable speed.

rameters, Eq. (12). Let us call the result of such calculations "*ab initio* SD profile". Another profile corresponding to the quadratic approximation for $\Gamma(z)$ using the aforementioned way to determine Γ_0 and Γ_2 parameters (Eqs. (20,21)) will be called the "qSD profile". Let us also calculate the speed-independent "SI profile" derived from the latter but setting $\Gamma_2 = \Delta_2 = Y_2 = 0$. This profile is, in fact, nothing but the VVWLM profile. The *ab initio* SD, qSD and SI profiles share the same line intensity. The differences between *ab initio* SD profiles and the two other profiles for the R(0) and R(1) lines are shown in Fig. 18. For comparison we present in this figure the residual of fitting the qSDVVWLM profile to the *ab initio* SD profile for the case when all parameters of the quadratic approximations for $\Gamma(z)$, $\Delta(z)$, $Y(z)$ and line intensity I are free.

At first glance, the result is astonishing: The profile using the commonly accepted quadratic approximation (Eq. (13)) reproduces the "real" (*ab initio*) one not much better than the SI profile. However, the residual of fitting the qSDVVWLM profile to the "real" one is about two orders of magnitude smaller, which evidences that the model itself is not so bad and can be really considered as an improvement of SI models. Note that similar fitting of the VVWLM profile with all free parameters to the *ab initio* one confirms that the aforementioned improvement constitutes about an order of magnitude (fit quality is 1500 and 1300 for the R(0) and R(1) lines, respectively). At this point we would like to remind the readers about the well-known difference between the "*ad hoc*" constant value of collisional line width Γ_V obtained from fitting a SI model and a "physically grounded definition" of the line half width $\Gamma_0 =< \Gamma(\upsilon) >$ and related Γ_2 parameter describing the speed-dependence of the collisional relaxation rate (see e.g. Koshelev et al.[62]). Our trial clearly demonstrates that the improvement in the line shape representation can be achieved only if both Γ_0 and Γ_2 are considered as efficient (or *ad hoc*) parameters of the qSD model[64]. It supplies from 5 to 6 times better description of the *ab initio* profiles than any other way of retrieving Γ_0 and Γ_2 parameters from the theoretically calculated dependence $\Gamma(\upsilon)$. A better representation of the line by the SI profile is the result of a poor fit of the quadratic function Eq. (13) to the real SD of collisional cross-section (Fig. 17). This fact indicates the potential problem of populating spectroscopic databases by calculated γ_0 and γ_2 coefficients, which can lead to worsening of the observed spectra modeling in comparison with the use of the SI approach.

This trial gives an easy possibility of quantitative evaluation of the impact of the SD in the first-order line mixing effect. The maximal relative difference between our *ab initio* SD profile and the same profile with the replacement of $Y(z)$ by Y_0 is smaller than $1.5 \cdot 10^{-4}$ for both R(0) and R(1) lines. Thus, a SNR of more than 7000 is requested to reveal the effect at pressures near 1000 Torr.

The trial reveals also a proper way of comparing experimentally determined collisional line shape coefficients responsible for the SD effect and their theoretical analogs: the same SD line shape model function should be fitted to the experimental recordings and to the general line shape profile (Eq. (12)) with theoretically calculated parameters $X(\upsilon)$. The resulting coefficients of the model are presented in Table 7 as *ab initio* data together with statistical uncertainty of the fit.

Further comparison of our *ab initio* results with qualitative theoretical approaches related in particular to the temperature dependence of collisional broadening is given in Appendix.

5 Conclusions

As a result of the analysis of the obtained experimental recordings, a complete set of spectroscopic parameters necessary for modeling the spectrum of a mixture of CO with Ar in the pressure range from millitorrs to several atmospheres at room temperature has been obtained, meeting high modern standards in terms of accuracy.

The use of spectrometers differing in the principle of operation and the range of operating pressures allows us to identify and minimize systematic measurement errors and increases the reliability of the obtained spectral line shape parameters.

The resulting set of collisional parameters is in excellent agreement with the results of quantum dynamical calculations based on *ab initio* intermolecular interaction potentials (up to the minor uncertainty associated with the choice between two competing potentials).

Numerical modeling of the spectrum in the vicinity of the center of the collisionally-broadened line on the basis of the results of *ab initio* calculations using generally accepted theoretical profiles, revealed a potential problem associated with filling the spectroscopic databases with theoretical coefficients for the quadratic speed-dependence model.

The use of the resonator spectrometer for CO spectrum recordings at pressures of broadening gas up to 2 atmospheres made it possible to identify potential manifestations of problems in modeling the spectrum using the traditional approach based on the impact approximation and the approximation of binary collisions.

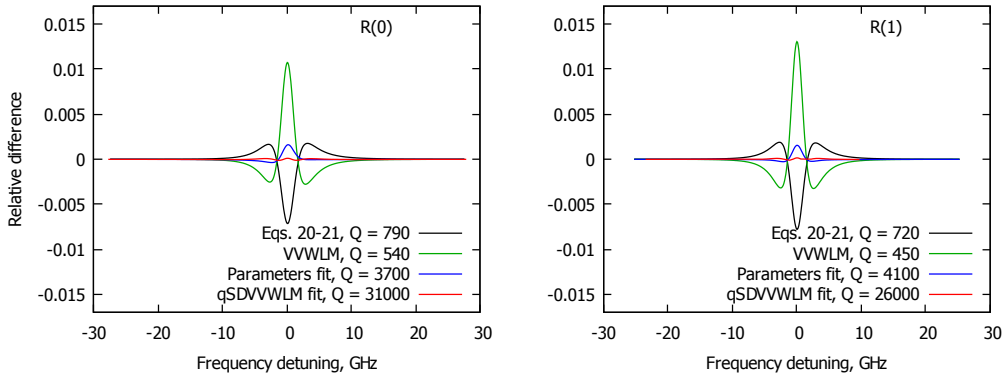

Fig. 18 Differences between *ab initio* profiles (Eq. (12)) of the R(0) and R(1) lines calculated at 297.5 K, 1000 Torr and various models: qSD-profile with X_0 and X_2 parameters calculated using Eq. (21) from *ab initio* dependences (black), the same but both X_0 and X_2 are retrieved from fitting Eq. (13) to *ab initio* $X(\upsilon)$ data (blue), VVWLM (or SI) profile (green), and fitted qSDVVWLM profile with all free parameters (red). See text for details.

In particular, the agreement of the measured interference coefficient of the R(0) line with the results of *ab initio* calculations and a significant discrepancy of similar data for the R(1) line indicates a possible violation of the impact approximation, manifested in a faster decay of the far wings of the lines with large detuning from the center. In addition, the observed spectrum cannot be represented as a traditional sum of the collisionally-broadened resonant lines of the CO monomer. The spectrum is located on a non-resonant pedestal that grows quadratically with frequency and possesses gas pressure dependences characteristic for the continuum. This indicates its possible bimolecular origin and opens up attractive prospects for further study of the spectrum.

Author Contributions

M. Yu. Tretyakov — conceptualization, writing — review & editing, supervision; E. A. Serov — formal analysis, vizualization, writing — original draft; D. S. Makarov — software, formal analysis, writing — original draft; I. N. Vilkov — investigation, data curation, resources; G. Yu. Golubiatnikov — investigation, data curation, resources, T. A. Galanina — investigation, data curation, resources, M. A. Koshelev — supervision, data curation, methodology, A. A. Balashov — investigation, data curation, A. A. Simonova — investigation, data curation; F. Thibault — methodology, software, formal analysis.

Conflicts of interest

There are no conflicts to declare.

Acknowledgements

Experimental data from RAD and video spectrometers were obtained with support from the Russian State Project 0030-2021-0016. Measurements of the R(1) line at elevated pressures with the resonator spectrometer and joint analysis of all data were performed within the RSF project 22-17-00041. SA acknowledges support from the Ministry of Science and Higher Education of the Russian Federation, project No. 121031500297-3.

Appendix

In this appendix we discuss the temperature dependence of the collisional broadening of the R(0) and R(1) CO lines, which was not experimentally studied in this work but was calculated *ab initio*. In particular, we continue the comparison of *ab initio* results with traditional analytical theoretical modeling of collisional effects, taking into account an intermolecular interaction potential V.

Let us assume that for the attractive (long range) part of the potential $V(R) \propto R^{-N}$, where R is the distance between colliding molecules. Then, considering only this part of the potential, it can be shown (see, e.g., Eq. (13.66) from Townes[41] and Pickett[54]) that the exponent value in $\Gamma(\upsilon_r) \propto \upsilon_r^n$ (Section 4) can be evaluated as

$$n = (N-3)/(N-1). \tag{22}$$

Note that on this basis the quadratic SD approximation ($n = 2$) leads to an unphysical result $N = -1$ (the interaction increases with increasing distance). Fortunately the model of Berman leading to Eq. (19) is valid for $N > 1.5$. Recall that we obtained $n = 0.44$ and, therefore, $N = 4.57$ in a good agreement with $N = 4.6$ reported for the R(0) line of the fundamental band for ^{13}CO molecule in Ar bath[65]. This value seems reasonable because the isotropic part of the CO–Ar potential is expected to be close to the Lennard — Jones 12–6 model and, thus, for large R the main contribution should scale as the dispersion interaction $\propto R^{-6}$.

We analyzed the long range part of selected angular curves of the interaction potential[36] (the most informative part of the curves is shown in the upper panel of Fig. 19), which was used in this work for the R(0) and R(1) parameters determination.

The lower panels of the figure present results of fitting the function $y(R) = a/(R-b)^N$ to the attractive wing of the potential in the most characteristic cases corresponding to three orientations of the CO molecule relative to Ar atom (characterized by angle θ). First of all, it shows that the wing cannot be accurately described by the "power law". However, the best result is obtained for $N = 6.4$ (above 5 Å the deviation is less than 0.1 cm^{-1}). It is worth mentioning that almost the same result is obtained

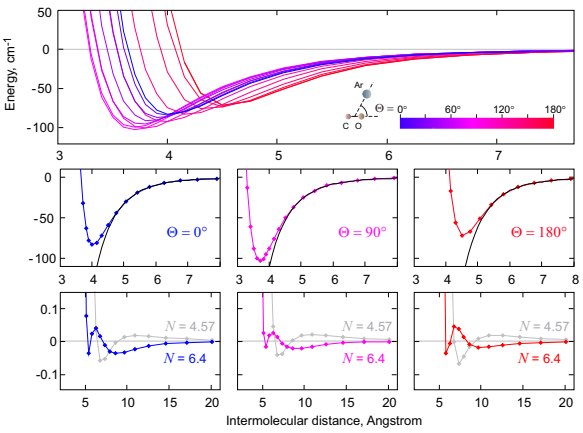

Fig. 19 CO–Ar interaction potential[36] for the C–O bond length of 1.132 Å and different orientations of CO relative to Ar (upper panel), its three upmost characteristic cases (middle row) and results of fitting to them the function $y(R) = a/(R-b)^N$ with $N = 6.4$ (in black in the middle row and in corresponding colour in the lower row) and 4.57 (in gray, lower row). See text for details.

by fitting the isotropic component of the potential (defined as $V_0(R) = \frac{1}{2}\int_0^\pi V(R,\theta)\sin\theta d\theta$). In this case, the best fit of the power law is obtained for $N = 6.3$ but $N = 6.4$ gives almost the same fit quality. Note also that adjusting of the numerical coefficients of an assumed Lennard-Jones *M*-*N* potential to the same data gives values of N within $6.5-6.55$ depending of different weighting of points. The result of the simulation of the power law function with the fixed value of $N = 4.57$ is shown in the lowest panels of Fig. 19. It reveals a quite comparable quality of the fit of the long range part of the potential, although for larger R.

The temperature dependence of the pressure broadening coefficient is derived starting from $\Gamma(\upsilon_r) \propto \upsilon_r{}^n$. The temperature dependence of υ_r is determined by the MB distribution but for the approximate/qualitative estimations it is common to adopt the temperature dependence of the most probable relative speed $\bar{\upsilon}_r \propto T^{\frac{1}{2}}$. Since $\gamma = \Gamma/p$ and $p \propto T^{-1}$, one obtains $\gamma(T) \propto T^{\frac{n}{2}-1}$ [41,54].

Moreover, it can be shown that this relation is rigorous and can be derived analytically. Making the link with an assumed long range interaction $V(R) \propto R^{-N}$ and Eq. (22) leads to a temperature dependence of $\gamma(T) \propto T^{-\frac{N+1}{2N-2}}$ [41,54,59,61]. For $N = 4.57$ the value of the temperature exponent is –0.78. The commonly used power law function $\gamma(T) = \gamma(T_0)(T/T_0)^{-0.78}$ with $T_0 = 297$ K is plotted in Fig. 20 together with the *ab initio* data for the R(0) and R(1) lines, demonstrating excellent agreement of the analytically derived temperature dependence with the *ab initio* data within a very broad $10-700$ K interval. The relative deviation of points from lines is less than 0.1 %. We stress that no adjustment was used in the plot. Note also that the use of the aforementioned (Section 4) fitted n values of 0.428 and 0.469 for the R(0) and R(1) lines, respectively, does not notably improve the agreement.

At room temperature, the broadening of R(J) lines mainly comes from the short range part of the CO–Ar interaction potential because the relative kinetic energy exceeds the potential well depth by about a factor of 3. However, it is well known that low J values are more sensitive to the long range part than high J values. This is probably the reason why this simple analytical approach for calculating the broadening temperature dependence works quite well for the R(0) and R(1) lines over a large temperature range.

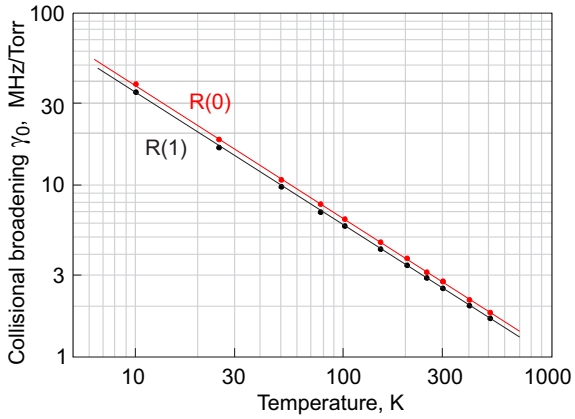

Fig. 20 *Ab initio* data on collisional broadening coefficient for the R(0) and R(1) lines of CO by pressure of Ar (red and black points, respectively) versus temperature and corresponding power law functions with the exponent value of -0.78 (solid lines). See text for details.

Notes and references

1 J.-M. Hartmann, C. Boulet and D. Robert, *Collisional effects on molecular spectra*, Elsevier, Amsterdam, 2008.

2 J.-M. Hartmann, H. Tran, R. Armante, C. Boulet, A. Campargue, F. Forget, L. Gianfrani, I. Gordon, S. Guerlet, M. Gustafsson, J. T. Hodges, S. Kassi, D. Lisak, F. Thibault and G. C. Toon, *J. Quant. Spectrosc. Radiat. Transfer*, 2018, **213**, 178–227.

3 S. A. Clough, F. X. Kneizys and R. W. Davies, *Atmos. Res.*, 1989, **23**, 229–241.

4 L. Frommhold, *Collision-induced absorption in gases*, Cambridge University Press, 2006.

5 D. E. Stogryn and J. O. Hirschfelder, *J. Chem. Phys.*, 1959, **31**, 1531–1545.

6 A. A. Vigasin, in *Bimolecular absorption in atmospheric gases*, ed. C. Camy-Peyret and A. A. Vigasin, Kluwer Academic Publishers, London, 2003, p. 23.

7 M. Yu. Tretyakov, E. A. Serov, M. A. Koshelev, V. V. Parshin and A. F. Krupnov, *Phys. Rev. Lett.*, 2013, **110**, 093001.

8 E. A. Serov, M. A. Koshelev, T. A. Odintsova, V. V. Parshin and M. Yu. Tretyakov, *Phys. Chem. Chem. Phys.*, 2014, **16**, 26221–26233.

9 K. P. Shine, A. Campargue, D. Mondelain, R. A. McPheat, I. V. Ptashnik and D. Weidmann, *J. Mol. Spectrosc.*, 2016, **327**, 193–208.

10 T. A. Odintsova, M. Yu. Tretyakov, A. O. Zibarova, O. Pirali, P. Roy and A. Campargue, *J. Quant. Spectrosc. Radiat. Transfer*, 2019, **227**, 190–200.

11 A. A. Vigasin, Y. I. Baranov and G. V. Chlenova, *J. Mol. Spectrosc.*, 2002, **213**, 51–56.

12 D. V. Oparin, N. N. Filippov, I. M. Grigoriev and A. P. Kouzov, *J. Quant. Spectrosc. Radiat. Transfer*, 2017, **196**, 87–93.
13 T. A. Odintsova, E. A. Serov, A. A. Balashov, M. A. Koshelev, A. O. Koroleva, A. A. Simonova, M. Yu. Tretyakov, N. N. Filippov, D. N. Chistikov, A. A. Finenko, S. E. Lokshtanov, S. V. Petrov and A. A. Vigasin, *J. Quant. Spectrosc. Radiat. Transfer*, 2021, **258**, 107400.
14 E. A. Serov, A. A. Balashov, M. Yu. Tretyakov, T. A. Odintsova, M. A. Koshelev, D. N. Chistikov, A. A. Finenko, S. E. Lokshtanov, S. V. Petrov and A. A. Vigasin, *J. Quant. Spectrosc. Radiat. Transfer*, 2020, **242**, 106774.
15 W. M. Elsasser, *Physical Review*, 1938, **53**, 768–768.
16 E. A. Serov, T. A. Odintsova, M. Yu. Tretyakov and V. E. Semenov, *J. Quant. Spectrosc. Radiat. Transfer*, 2017, **193**, 1–12.
17 M. Birk, G. Wagner, J. Loos and K. P. Shine, *J. Quant. Spectrosc. Radiat. Transfer*, 2020, **253**, 107134.
18 T. A. Odintsova, A. O. Koroleva, A. A. Simonova, A. Campargue and M. Yu. Tretyakov, *J. Molec. Spectrosc.*, 2022, **386**, 111603.
19 A. O. Koroleva, T. A. Odintsova, M. Yu. Tretyakov, O. Pirali and A. Campargue, *J. Quant. Spectrosc. Radiat. Transfer*, 2021, **261**, 107486.
20 S. V. Ivanov, *J. Quant. Spectrosc. Radiat. Transfer*, 2016, **177**, 269–282.
21 H. Tran, G. Li, V. Ebert, and J.-M. Hartmann, *J. Chem. Phys.*, 2017, **146**, 194305.
22 G. Winnewisser, S. P. Belov, T. Klaus and R. Schieder, *J. Mol. Spectrosc.*, 1997, **184**, 468–472.
23 H. Mader, A. Guarnieri, J. Doose, N. Nissen, V. N. Markov, A. M. Shtanyuk, A. F. Andrianov, V. N. Shanin and A. F. Krupnov, *J. Mol. Spectrosc.*, 1996, **180**, 183–187.
24 V. N. Markov and H. Mader, *J. Mol. Spectrosc.*, 2001, **205**, 350–352.
25 K. Yamada and H. Abe, *J. Mol. Spectrosc.*, 2003, **217**, 87–92.
26 J.-M. Colmont, L. Nguyen, F. Rohart and G. Wlodarczak, *J. Mol. Spectrosc.*, 2007, **246**, 86–97.
27 A. F. Seleznev, G. V. Fedoseev, M. A. Koshelev and M.Yu. Tretyakov, *J. Quant. Spectrosc. Radiat. Transfer*, 2015, **161**, 171–179.
28 A. Predoi-Cross, K. Esteki, H. Rozario, H. Naseri, S. Latif, F. Thibault, V. Malathy Devi, M. Smith and A. Mantz, *J. Quant. Spectrosc. Radiat. Transfer*, 2016, **184**, 322–340.
29 A. Predoi-Cross, J. P. Bouanich, D. C. Benner, A. D. May and J. R. Drummond, *J. Chem. Phys.*, 2000, **113**, 158–168.
30 E. A. Serov, N. Stolarczyk, D. S. Makarov, I. N. Vilkov, G. Yu. Golubiatnikov, A. A. Balashov, M. A. Koshelev, P. Wcisło, F. Thibault and M. Yu. Tretyakov, *J. Quant. Spectrosc. Radiat. Transfer*, 2021, **272**, 107807.
31 S. Hess, *Physica*, 1972, **61**, 80–94.
32 J. Schaefer and W. Köhler, *Physica A*, 1985, **129**, 469.
33 L. Demeio, S. Green and L. Monchick, *J. Chem. Phys.*, 1995, **102**, 9160–9166.
34 F. Thibault, K. Patkowski, P. S. Żuchowski, H. Jóźwiak, R. Ciuryło and P. Wcisło, *J. Quant. Spectrosc. Radiat. Transfer*, 2017, **202**, 308.
35 Y. Sumiyoshi and Y. Endo, *J. Chem. Phys.*, 2015, **142**, 024314.
36 G. Kowzan, H. Cybulski, P. Wcisło, M. Słowiński, A. Viel, P. Masłowski and F. Thibault, *Phys. Rev. A*, 2020, **102**, 012821.
37 G. Golubiatnikov, S. P. Belov, I. I. Leonov, A. F. Andriyanov, I. I. Zinchenko, A. V. Lapinov, V. N. Markov, A. P. Shkaev and A. Guarnieri, *Radiophys. Quantum El.*, 2014, **56**, 599–609.
38 G. Yu. Golubiatnikov, S. P. Belov and A. V. Lapinov, *Radiophys. Quantum El.*, 2017, **59**, 715–726.
39 N. Ngo, D. Lisak, H. Tran and J.-M. Hartmann, *J. Quant. Spectrosc. Radiat. Transfer*, 2013, **129**, 89–100.
40 M. Yu. Tretyakov and A. F. Krupnov, *J. Mol. Spectrosc.*, 1995, **172**, 205—210.
41 C. H. Townes and A. L. Schawlow, *Microwave Spectroscopy*, New York : McGraw-Hill, 1955.
42 C. A. Burrus and W. Gordy, *Phys. Rev.*, 1954, **93**, 897–898.
43 I. E. Gordon, L. S. Rothman, R. J. Hargreaves, R. Hashemi, E. V. Karlovets, F. M. Skinner, E. K. Conway, C. Hill, R. V. Kochanov, Y. Tan, P. Wcisło, A. A. Finenko, K. Nelson, P. F. Bernath, M. Birk, V. Boudon, A. Campargue, K. V. Chance, A. Coustenis, B. J. Drouin, J.-M. Flaud, R. R. Gamache, J. T. Hodges, D. Jacquemart, E. J. Mlawer, A. V. Nikitin, V. I. Perevalov, M. Rotger, J. Tennyson, G. C. Toon, H. Tran, V. G. Tyuterev, E. M. Adkins, A. Baker, A. Barbe, E. Canè, A. G. Császár, A. Dudaryonok, O. Egorov, A. J. Fleisher, H. Fleurbaey, A. Foltynowicz, T. Furtenbacher, J. J. Harrison, J.-M. Hartmann, V.-M. Horneman, X. Huang, T. Karman, J. Karns, S. Kassi, I. Kleiner, V. Kofman, F. Kwabia–Tchana, N. Lavrentieva, T. Lee, D. Long, A. Lukashevskaya, O. Lyulin, V. Makhnev, W. Matt, S. Massie, M. Melosso, S. Mikhailenko, D. Mondelain, H. Müller, O. Naumenko, A. Perrin, O. Polyansky, E. Raddaoui, P. Raston, Z. Reed, M. Rey, C. Richard, R. Tóbiás, I. Sadiek, D. Schwenke, E. Starikova, K. Sung, F. Tamassia, S. Tashkun, J. Vander Auwera, I. Vasilenko, A. Vigasin, G. Villanueva, B. Vispoel, G. Wagner, A. Yachmenev and S. Yurchenko, *J. Quant. Spectrosc. Radiat. Transfer*, 2022, **277**, 107949.
44 A. Henry, D. Hurtmans, M. Margottin-Maclou and A. Valentin, *J. Quant. Spectrosc. Radiat. Transfer*, 1996, **56**, 647–671.
45 A. F. Krupnov, in *Modern Aspects of Microwave Spectroscopy*, ed. G. W. Chantry, Academic Press, L, 1979, pp. 217–256.
46 M. Yu. Tretyakov, M. A. Koshelev, D. S. Makarov and M. V. Tonkov, *Instruments and Experimental Techniques*, 2008, **51**, 78–88.
47 M. A. Koshelev, A. I. Tsvetkov, M. V. Morozkin, M. Yu. Glyavin and M. Yu. Tretyakov, *J. Mol. Spectrosc.*, 2017, **331**, 9–16.
48 G. Yu. Golubiatnikov, M. A. Koshelev, A. I. Tsvetkov, A. P. Fokin, M. Yu. Glyavin and M. Yu. Tretyakov, *IEEE Transactions on Terahertz Science and Technology*, 2020, **10**, 502–512.
49 D. S. Makarov, I. N. Vilkov, M. A. Koshelev, A. A. Aderkina and M. Yu. Tretyakov, *Radiophys. Quantum El.*, 2018, **60**, 808–823.
50 M. A. Koshelev, I. I. Leonov, E. A. Serov, A. I. Chernova, A. A.

Balashov, G. M. Bubnov, A. F. Andriyanov, A. P. Shkaev, V. V. Parshin, A. F. Krupnov and M. Yu. Tretyakov, *IEEE Transactions on Terahertz Science and Technology*, 2018, **8**, 773–783.

51 P. W. Rosenkranz, *IEEE Trans. Antennas Propag.*, 1975, **23**, 498–506.

52 C. Luo, R. Wehr, J. R. Drummond, A. D. May, F. Thibault, J. Boissoles, J. M. Launay, C. Boulet, J.-P. Bouanich and J.-M. Hartmann, *J. Chem. Phys.*, 2001, **115**, 2198–2206.

53 R. Hashemi, I. E. Gordon, E. M. Adkins, J. T. Hodges, D. A. Long, M. Birk, J. Loos, C. D. Boone, A. J. Fleisher, A. Predoi-Cross and L. S. Rothman, *J. Quant. Spectrosc. Radiat. Transfer*, 2021, **271**, 107735.

54 H. M. Pickett, *J. Chem. Phys.*, 1980, **73**, 6090.

55 J. Tennyson, P. F. Bernath, A. Campargue, A. G. Császár, L. Daumont, R. R. Gamache, J. T. Hodges, D. Lisak, O. V. Naumenko, L. S. Rothman, H. Tran, N. F. Zobov, J. Buldyreva, C. D. Boone, M. D. D. Vizia, L. Gianfrani, J.-M. Hartmann, R. A. McPheat, D. Weidmann, J. M. Murray, N. H. Ngo and O. L. Polyansky, *Pure and Applied Chemistry*, 2014, **86**, 1931–1943.

56 H. J. Liebe, *Int. J. Infrared Mill. Waves*, 1989, **10**, 631–650.

57 A. I. Meshkov and F. C. De Lucia, *J. Quant. Spectrosc. Radiat. Transfer*, 2007, **108**, 256–276.

58 T. A. Odintsova, E. A. Serov, A. A. Balashov, M. A. Koshelev, A. O. Koroleva, A. A. Simonova, M. Yu. Tretyakov, N. N. Filippov, D. N. Chistikov, A. A. Finenko, S. E. Lokshtanov, S. V. Petrov and A. A. Vigasin, *J. Quant. Spectrosc. Radiat. Transfer*, 2021, **258**, 107400.

59 J. Ward, J. Cooper and E. W. Smith, *J. Quant. Spectrosc. Radiat. Transfer*, 1974, **14**, 555–590.

60 R. Wehr, A. Vitcu, R. Ciuryło, F. Thibault, J. R. Drummond and A. D. May, *Phys. Rev. A*, 2002, **66**, 062502.

61 P. Berman, *J. Quant. Spectrosc. Radiat. Transfer*, 1972, **12**, 1331–1342.

62 M. A. Koshelev, M. Yu. Tretyakov, F. Rohart and J.-P. Bouanich, *J. Chem. Phys.*, 2012, **136**, 124316.

63 M. A. Koshelev, I. N. Vilkov, D. S. Makarov, M. Yu. Tretyakov, B. Vispoel, R. R. Gamache, D. Cimini, F. Romano and P. W. Rosenkranz, *J. Quant. Spectrosc. Radiat. Transfer*, 2021, **262**, 107472.

64 N. Ngo, H. Lin, J. Hodges and H. Tran, *J. Quant. Spectrosc. Radiat. Transfer*, 2017, **203**, 325–333.

65 A. W. Mantz, F. Thibault, J. L. Cacheiro, B. Fernandez, T. B. Pedersen, H. Koch, A. Valentin, C. Claveau, A. Henry and D. Hurtmans, *J. Mol. Spectrosc.*, 2003, **222**, 131–141.